UCRL-17872

c.2

University of California

Ernest O. Lawrence Radiation Laboratory

THE MICROSTRUCTURE AND PLANE STRAIN FRACTURE TOUGHNESS OF HIGH STRENGTH ALUMINUM ALLOYS

Peter John Guest
(M. S. Thesis)

October 1967

TWO-WEEK LOAN COPY

This is a Library Circulating Copy which may be borrowed for two weeks. For a personal retention copy, call Tech. Info. Division, Ext. 5545

UCRL-17872 c.2

DISCLAIMER

This document was prepared as an account of work sponsored by the United States Government. While this document is believed to contain correct information, neither the United States Government nor any agency thereof, nor the Regents of the University of California, nor any of their employees, makes any warranty, express or implied, or assumes any legal responsibility for the accuracy, completeness, or usefulness of any information, apparatus, product, or process disclosed, or represents that its use would not infringe privately owned rights. Reference herein to any specific commercial product, process, or service by its trade name, trademark, manufacturer, or otherwise, does not necessarily constitute or imply its endorsement, recommendation, or favoring by the United States Government or any agency thereof, or the Regents of the University of California. The views and opinions of authors expressed herein do not necessarily state or reflect those of the United States Government or any agency thereof or the Regents of the University of California.

UCRL-17872

UNIVERSITY OF CALIFORNIA

Lawrence Radiation Laboratory
Berkeley, California

AEC Contract No. W-7405-eng-48

THE MICROSTRUCTURE AND PLANE STRAIN FRACTURE TOUGHNESS OF HIGH STRENGTH ALUMINUM ALLOYS

Peter John Guest

(M.S. Thesis)

October 1967

TABLE OF CONTENTS

ABSTRACT

I LIST OF SYMBOLS 1

II INTRODUCTION 2

III FRACTURE TOUGHNESS 4

IV MATERIAL 9

V EXPERIMENTAL PROCEDURE 10

A. Specimen Design and Instrumentation 10

B. Mechanical Testing 11

C. Compliance Analysis 11

D. Evaluation of True Stress-True Strain Properties 12

E. Heat Treatment 13

F. Mechanical Stabilization 14

VI EXPERIMENTAL RESULTS AND DISCUSSION 15

A. General 15

B. Effect of Specimen Size 16

C. Effect of Heat Treatment 17

VII SUMMARY AND CONCLUSIONS 21

ACKNOWLEDGMENTS 23

REFERENCES 24

TABLES 25

FIGURE CAPTIONS 34

FIGURES 37

THE MICROSTRUCTURE AND PLANE STRAIN FRACTURE TOUGHNESS OF HIGH STRENGTH ALUMINUM ALLOYS

Peter John Guest

Inorganic Materials Research Division, Lawrence Radiation Laboratory, Department of Mineral Technology, College of Engineering, of the University of California, Berkeley, California

ABSTRACT

The plane-strain fracture toughness of precipitation hardening high strength 7075-aluminum alloy has been determined in the fully precipitation hardened condition (38 ksi-$\sqrt{\text{in}}$) and compared with the overaged and underaged conditions at predetermined stress levels less than the yield strength. Plane-strain fracture toughness values were determined using the "pop-in" technique employing single edge notched large and small type specimens. The results show that the plane-strain fracture toughness was markedly improved for both underaged (61 ksi-$\sqrt{\text{in}}$) and overaged conditions (47 ksi-$\sqrt{\text{in}}$) accompanied by a corresponding minimal loss in yield strength. The underaged condition exhibited higher toughness than the overaged condition at equivalent yield strength levels. The work required to cause crack propagation was found to increase considerably for underaging and overaging, with a larger increase for the underaged condition, over the fully precipitation hardened condition. The plane-strain fracture toughness was found to increase with increasing strain hardening exponent.

I. LIST OF SYMBOLS

K	Stress intensity parameter describing the local increase of elastic stress field ahead of the crack. The value of K at instability is referred to as the fracture toughness and is expressed as psi-in$^{1/2}$.
I	Subscript denoting first or opening mode of fracture. Referred to as plane-strain condition.
C	Subscript denoting critical value of any parameter.
σ	Net section average stress, psi (based on notched or unnotched area).
σ_{YS}	Yield stress at 0.20 percent offset, psi.
σ_{UTS}	Ultimate tensile stress, psi.
σ_{FS}	Fracture stress, psi.
σ_T	True stress, psi.
B	Specimen thickness, in.
W	Specimen width, in.
n	Strain hardening exponent (in $\sigma_T = k\epsilon^n$)
k	Strength coefficient.
ϵ	Strain, in/in.
$\mathcal{G}$	Strain energy release rate, in-lb/in^2.
a	1/2 crack length, in.
ν	Poisson's ratio.
E	Young's modulus
P	Applied load, lbs.
ϵ_T	True strain, in/in.

II. INTRODUCTION

The development of good fracture toughness has been the desired result of alloys design. Since fracture toughness is considered an important fundamental material property used in design, the enhancement of this property through such metallurgical factors as heat treatment was initiated.

The requirement for high strength materials with an efficient strength-to-density index for use in aircraft has accentuated the importance of fracture toughness. High strength materials at high stress levels have been found to behave in a brittle manner in the presence of small flaws which are initially present in the material. As a result, service failure sometimes occurs by brittle fracture rather than by yielding and distortion and at stresses well below the design stress, usually based on the yield strength of the material. Fracture toughness is the material characteristic used as a measure of a materials resistance to fracture in the presence of flaws, specifically the resistance of a material to crack propagation.

The fracture toughness (as measured by a critical value of K) decreases as the specimen thickness increases through the range encompassing the fracture-mode transition from a shear failure to a flat fracture. At the thickness where the elastic constraint is sufficiently large so that the ductile-brittle transition is complete, further increases of specimen thickness produces no additional decrease in the fracture toughness. This condition is described as being essentially plane-strain and the value of fracture toughness at which instability occurs is designated at K_{IC}.

Because of its recognition as a useful design parameter, K_{IC} has been

measured in the present study to obtain the effect of artificial aging on the fracture characteristics of 7075-aluminum.

The present investigation has shown the importance of using the fracture mechanics approach in the development of reliable high strength alloys.

III. FRACTURE TOUGHNESS

The discrepancy between the experimental fracture strength of crystals and theoretical cohesive strength was first explained by the Griffith theory. This theory, although applied originally to glass, has been adapted by others to explain metal fracture.

Griffith postulated that a crack will propagate when the decrease in elastic strain energy is at least equal to the energy required to create a new crack surface. This concept can be used to determine the magnitude of the tensile stress which will just cause a crack of a certain size to propagate in a brittle manner.

For a plate which is very thin so as to be in a condition of plane stress, the Griffith equation is given by

$$\sigma = \sqrt{\frac{2E\gamma}{\pi a}}$$

where σ is the applied tensile stress normal to a crack of length, 2a, having a surface tension of γ and E is the modulus of elasticity.

For a plate that is thick compared with the length of the crack, that is, plane strain, the Griffith equation is given by

$$\sigma = \sqrt{\frac{2E\gamma}{(1-\nu^2)\pi a}}$$

where ν is Poisson's ratio.

These equations predict the stress needed to propagate a crack through a brittle solid.

Irwin extended the Griffith theory into the area of fracture

mechanics. The objective was to find a reliable design criterion for predicting the stress at which rapidly propagating fractures will occur. This is essentially a macroscopic theory that is concerned with cracks of the order of tenths of an inch in length. The quantity of interest is the crack extension force or the elastic strain energy release rate. The strain energy release rate, $\mathcal{G}$, measured in units of in-lbs/in^2 is the quantity of stored elastic strain energy released from a cracking specimen as the result of the extension of an advancing crack by a unit area. When $\mathcal{G}$ reaches a critical value $\mathcal{G}_C$, the crack will propagate rapidly. $\mathcal{G}_C$ is termed the fracture toughness in the energy balance model and is the energy which is absorbed in local plastic flow and cleavage in creating a unit area of fracture surface. $\mathcal{G}_C$ appears to be a basic material properly independent of plate size effects, yet dependent upon composition, microstructure, temperature, and rate of loading.

To measure $\mathcal{G}_C$, it is necessary to have a valid expression for $\mathcal{G}$ in terms of crack dimensions, specimen geometry and the normal applied stress. The specimen is then loaded until a stress is reached at which the crack, which is initially present in the specimen, propagates rapidly. The calculated value of $\mathcal{G}$ for this condition is then $\mathcal{G}_C$. For a crack of length 2a in an infinitely wide plate the relationship between the stress and $\mathcal{G}$ is given by

$$\sigma = \sqrt{\frac{\mathcal{G} E}{\pi a}} \quad . \qquad \text{(Ref. 12)}$$

The energy release rate can be related to the stress pattern near the crack tip as follows,

$$\sigma_Y = \frac{K}{(2\pi r)^{1/2}}$$

where σ_Y is the stress normal to the crack tip and r is the distance in front of the tip in the x direction. (See Fig. 1.) K is a function only of crack size, loads and shape of the part and is called the "stress intensity factor." K is a material characteristic and is referred to as the fracture toughness parameter in the stress intensity approach. $\mathcal{G}$ is related to K as follows

$$K = \sqrt{E\mathcal{G}} \quad \text{for plane stress, and}$$

$$K = \sqrt{\frac{E\mathcal{G}}{(1-\nu^2)}} \quad \text{for plane strain.}$$

It can also be shown that $K = \sigma\,(\pi a)^{1/2}$, showing the equivalence of crack length and applied stress.

The critical stress system under which failure occurs is characterized by K_C and $\mathcal{G}_C$. The following definitions using the stress intensity factor approach make the necessary distinctions between plane stress and plane strain.

K_{IC} is the stress intensity value at the onset of crack growth under plane strain.

K_C is the stress intensity value at the onset of crack growth under plane stress.

This concept of fracture toughness stems from the stress pattern ahead of the crack tip in a linear elastic material. Since a plastic zone usually exists in real materials, some correction for this must

be made. A plastic zone correction factor, r_y, can be added to the crack length a. The radius of this zone can be estimated by setting $\sigma_y = \sigma_{YS}$ in the yield strength of the material giving

$$r_y = \frac{1}{2\pi}\left(\frac{K}{\sigma_{YS}}\right)^2$$

Fracture occurs at the crack tip when a critical normal stress, $\sigma = \sigma_C$, is attained at a fixed distance r_C, then

$$K_{crit} = \sigma_C(2\pi r_C)^{1/2} \quad .$$

Fracture mechanics, as briefly outlined, provides a method to measure the brittle strength of a material.

The value of fracture toughness at which instability occurs can be determined by monitoring the crack growth to observe where "pop-in" occurs. The conditions of crack propagation during "pop-in" are assumed to be that of plane-strain. The determination of plane-strain fracture toughness by a sudden burst of crack propagation enables the use of smaller specimens.[1] A high degree of constraint can be achieved at the notch tip even though the size of the plastic zone approaches that of the specimen thickness. The extent of "pop-in" diminishes as the thickness is decreased until at some critical value of thickness, the constraint-relieving influence of the free faces of the specimen will extend through the thickness before the stress intensity reaches K_{IC}. This relief of constraint due to plastic deformation tends to suppress sudden crack propagation.

The value of K_{IC} can be determined by measuring the load at which "pop-in" occurs. Srawley and Brown[3] first observed that a sudden burst of crack growth at the plain-strain toughness level preceded slow crack growth under an increasing load.

Various methods for detecting the onset of crack propagation involve the measurement of crack opening displacement, electrical potential and stress wave emission. The method used in this research is that of displacement measurement at the crack opening.

IV. MATERIAL

A precipitation hardening aluminum alloy of the 7000 series, 7075, procured as commercially rolled plate in the T6 temper, was selected for this investigation. This alloy is composed of 5.6% Zn, 2.5% Mg, 1.6% Cu and 0.25% Cr. The temper designation (-T6) refers to a solution heat treating and artificial aging.

The engineering tensile properties of 7075-T6 in the as-received condition were observed to be well within the normal commercial specification requirements for these alloys. The yield strength (0.20% offset) and ultimate tensile strength was determined to be 77,000 psi and 84,000 psi respectively, and the elongation, 14%. A longitudinal direction (specimen axis) of the rolled structure was used in all mechanical tests.

V. EXPERIMENTAL PROCEDURE

A. Specimen Design and Instrumentation

The specimen design used was such that a minimum amount of plastic deformation occurred at the crack tip under the applied stress condition. This permitted evaluation of the fracture toughness without the necessity of a plastic zone correction factor.

The fracture plates used were of the single edge notched design recommended by the A.S.T.M. Committee E-24 on "Fracture Testing of Materials", published in the A.S.T.M. Standards, 1967. The dimensions are as shown in Figs. 2(a) and 2(b). The length of each type is sufficient to avoid interaction of pin hold stresses with the tensile stresses in the region of the notch. The specimens were pin loaded to assure good alignment. No yielding occurred around the pin holes. The thickness of the plates was such that the initial mode of failure under tension was the flat brittle type and the condition of failure indicated rapid plane-strain fracturing at the beginning of crack propagation, as shown in Fig. 4.

The tensile specimen designs were both made according to the A.S.T.M. Designation: E8-65T and are shown in Figs. 3(a) and 3(b).

Referring to Fig. 5, the crack opening displacement was measured between two fiducial points on opposite sides of the notch edge. The opening is related to the crack extension. The type of transducer used was a double cantilever beam gauge developed by Fisher and Srawley[2] and discussed by Srawley and Brown.[3] This instrument is suitable for the detection of "pop-in" and combines high sensitivity with linear output. The arms of the gauge were made from spring steel which has a good ratio

of yield strength to Young's modulus. The resistance strain gauges were epoxy resin bonded to the arms to form a bridge arrangement. Grooves in the ends of the cantilevers contact knife edges machined into the edge notched specimens on either side of the notch. This method of locating the gauge is satisfactory in that the gauge is positively positioned during testing. The output of the strain gauge was monitored continuously on a high speed strip chart recorder.

B. Mechanical Testing

The testing machine used was a "Materials Testing Systems" 300 Kip universal testing machine. The fracture specimens were loaded at a constant extension rate of 0.02 in/min. When sudden crack propagation occurred at "pop-ins", the applied load remained approximately constant. This is shown schematically in Fig. 4. For the large fracture plates, a two-channel strip chart recorder simultaneously recorded the crack opening displacement and load versus time. In addition, an x-y recorder recorded the load against extension. Figures 6 and 7 show the experimental arrangement including the compliance gauge. The tensile specimens were loaded in the same manner as the fracture plates at a rate of 0.02 in/min.

C. Compliance Analysis

The results of a compliance analysis performed by Sullivan[4] and reproduced in Fig. 8, were used in the determination of K_{IC} for the small fracture specimens. The compliance curve obtained by Sullivan was derived from experimental compliance measurements on specimens that were pin loaded in the W/3 position. The curve gives a value of γ which can be used to calculate K_{IC}:

$$K_{IC}^2 (1 - \nu^2) = \gamma \sigma^2 W$$

where γ is the value taken from the compliance curve corresponding to a_o/W.

The K_{IC} calibration used for the large fracture specimens by Gross et al.[5] and discussed by Srawley and Brown,[6,7] is reproduced in Fig. 9. This calibration curve was derived analytically by a collocation procedure for a specimen pin loaded through the centerline. In deriving this curve it was assumed that the tensile load is uniformly distributed across the width of the specimen at a distance from the crack not less than the width. The K_{IC} calibration for this case is represented by the following equation.

$$Y = \frac{K_{IC} BW}{Pa^{1/2}}$$

where Y is the value taken from the ordinate of the curve corresponding to a/W.

A more direct and more appropriate method for the determination of K_{IC} would be through a stress analysis of these specimens. This form of analysis is presently unavailable.

D. Evaluation of True Stress - True Strain Properties

Computer facilities including a CDC 6600 electronic data processing system using the common language, FORTRAN IV, were used in the evaluation of the true stress-true strain properties and the value of the strain hardening exponent, n.

The relationship, in which the strain hardening exponent is expressed, is as follows

$$\sigma_T = k \epsilon_T^n$$

where k is a constant. The exponent n can be evaluated in the following manner.

Taking logarithms of both sides gives

$$n \log \epsilon = \log \sigma_T - \log k$$

Differentiating and solving for n gives

$$n = \frac{d(\log \sigma_T)}{d(\log \epsilon)}$$

It is shown that the strain hardening exponent is equal to the slope of the log true stress-log true strain plot.

To compute n and k, points were taken from the load displacement curves at points beyond the yield stress and below the ultimate stress.

The output data or true stress-true strain properties were plotted along with log-log plots of the properties. Such plots are shown in Fig. 10 for reproduced plots.

E. Heat Treatment

The heat treatments consisted of overaging and underaging both fracture and tensile specimens for various times and temperatures to attain a desired yield stress.

Artificial aging and reheating time and temperature curves published by Anderson[8] for 7075 material were used as guides in the heat treatment. These curves are reproduced in Figs. 11 and 12.

The fracture plates and tensile specimens for series 1 and 3 were reheated from T-6 condition (overaged) at temperatures from 425°F to 325°F to a constant yield stress level of 60,000 psi. In all tests where specimens were underaged, they were first resolution heat treated at 870°F for 0.5 hours, the recommended treatment for 7075-T6. The aging temperature for the underaged specimens varied from 250°F to 300°F to obtain the same yield stress level.

Another series was carried out using small fracture plates and short gauge tensile specimens to attain a stress level of 66,000 psi. The underaging and overaging temperature ranges were the same as the aforementioned test series.

F. Mechanical Stabilization

To determine whether the effect of straining prior to or during aging influenced the tensile and, more particularly, the fracture properties, additional specimens were heat treated similar to series 2 where a constant yield stress level of 66,000 psi was desired. The deformation was effected by rolling at room temperature to approximately 1% strain in the thickness direction. The specimens were then stress relieved by heat treating for 15% of the prior overaging or underaging time at the same temperatures.

VI. EXPERIMENTAL RESULTS AND DISCUSSION

A. General

The results of this study are tabulated in Tables I through VIII. Table I summarizes the tensile and fracture properties of the 7075-T6 alloy in the fully precipitation hardened condition while Tables II through VIII show the properties after various overaging and underaging times and temperatures.

The test series number shown on each table heading refers to the specimen size (test series 1 for the large specimens and test series 2 and 3 for the small specimens) and a yield stress level chosen for the heat treatment (60,000 psi for test series 1 and 3 and 66,000 psi for test series 2).

Each table also includes the measured amount of external energy stored to K_{IC}. This energy was obtained by measuring the area beneath the load-displacement curve with a planimeter and represents the energy absorbed or stored by the specimen under the imposed loading conditions.

It is considered that external energy absorbed to K_{IC} should correlate with $\mathcal{G}_{IC}$ on physical grounds, however such correlation is difficult to establish mathematically. The equation expressing the energy balance during loading is as follows:

$$U_{total} = U_{strain\ energy} + U_{surface\ energy}$$

where the total energy U is that measured amount absorbed to K_{IC}.

Differentiating this with respect to crack length a gives

$$\frac{\partial U}{\partial a} = \frac{\partial U_{\text{strain E}}}{\partial a} + \frac{\partial U_{\text{surf. E}}}{\partial a}$$

and further,

$$\frac{\partial U_{\text{total}}}{\partial a} = \mathcal{G}_{IC} + \frac{\partial U_{\text{surf. E}}}{\partial a} = 0 \quad .$$

The load-displacement curves obtained for the fracture specimens are similar in many respects to a regular stress-strain curve. With reference to Fig. 13(b), the first part of the curve up to "pop-in" is a straight line representing elastic deformation within the specimen. The start of crack propagation is shown by a deviation from the straight line and corresponds to rapid crack growth (instability) at constant load. The point of deviation of the curve corresponds to the "pop-in" and indicates rapid plane-strain fracturing at the beginning of crack propagation. "Pop-in" can also be detected by an accompanying audible "click" as the crack rapidly propagates. The load corresponding to this point on the curve is used in calculating K_{IC}.

B. Effect of Specimen Size

In selecting a specimen size for K_{IC} measurements one of the obvious factors to be considered is the desired accuracy of the K_{IC} measurement. The size of the specimen, the accuracy of the expression used in calculating K_{IC} and the form of measurement effects this accuracy. In this study, the accuracy of the expressions for K_{IC} for the large and small single edge notched specimens obtained by a mathematical procedure of boundary collocation[5] and by the experimental compliance measurement[4] are very good and are believed by Srawley and Brown[2] to be of the order

± 1/2 percent when 2a/W is about 0.3 to 0.5. The measurements have been made with high accuracy due to the nature of the M.T.S. machine and the instrumentation. According to Srawley and Brown[2] the width-to-thickness ratio should be of the order of $4 \leq \frac{W}{B} \leq 8$ for single edge notched specimens, as were the specimens used in this study.

Referring to Table I, the fracture properties of the large and small type single edge notched specimens differ slightly although the corresponding tensile properties are comparable. The difference might be due to the loading conditions (load applied as $\frac{W}{2}$ for the large specimen and $\frac{W}{3}$ for the small specimen). The difference is reflected both in K_{IC} and in the value of external energy absorbed by K_{IC}. When the crack became unstable ("pop-in"), with the small fracture specimens, the effective net cross sectional area was reduced to such a degree that complete fracture occurred immediately. A characteristic audible "click" could be heard just prior to fracture in all cases. With the large fracture specimens loading continued beyond "pop-in" as further external energy was absorbed by the specimen until complete fracture occurred.

C. Effect of Heat Treatment

In Fig. 14, the plane-strain fracture toughness, K_{IC}, of 7075 for various aging treatments is plotted against the yield strength. As would be expected, the plane-strain fracture toughness is an inverse function of the yield strength. These data obtained for the 7075 in the T6 condition compare favorably with that published by investigators such as Carman, Armiento and Markus[9] and Campbell.[10] Generally, the band delineating the results for the overaged condition increases more with decreasing yield strength than those results for the overaged condition.

Hence, the relative improvement in the fracture toughness at high strength levels with little loss in yield strength is better achieved in the underaged condition.

The variations of K_{IC}/σ_{YS} with σ_{YS} are shown in Fig. 15. The slopes of the bands indicate that in each test series the underaged specimens have considerably better values of plane-strain fracture toughness and hence K_{IC}/σ_{YS} ratios at equivalent yield strengths than for the overaged specimens. The effect of cold rolling underaged specimens in test series 2, (a common way to counteract susceptibility to Stress Corrosion Cracking), reduced the K_{IC}/σ_{YS} ratio with σ_{YS} to the band of values for overaging. This indicates that the small amount of plastic deformation reduced the ability of these specimens to absorb energy while being loaded during the test.

In Fig. 16, K_{IC} is plotted as a function of the external energy absorbed to K_{IC}. The underaged specimens are shown to have a greater energy absorption capacity at higher values of K_{IC} than than the overaged specimens. Table V shows that with a 9% drop in the yield strength the work required to cause crack propagation is increased 110% and the plane-strain fracture toughness 35% for a typical series (test series 2) of underaged specimens. The loss in yield strength is significantly lower than the accompanying gain in K_{IC}, and is of little importance when attention in design practices is centered around the limiting flaw size.

The effect of plate size is recorded in Fig. 17, where the external energy absorbed to K_{IC}, is plotted as a function of the yield strength. The value of K_{IC} for the small size specimens in the overaged condition are lower than the value for the large size specimen (lower two bands). A similar effect was observed for the underaged condition (upper band).

The ability of the large size specimens, compared to the small, to absorb greater amounts of external energy per unit area is largely due to the variance in the loading conditions and hence in the contrasting stress patterns ahead of the advancing crack front. Of significance also is the more rapid increase with corresponding yield strength decrease in the amount of work needed to cause crack propagation for the underaged specimens compared to that for the averaged specimens.

It has been shown that the K_{IC} values and amount of external energy absorbed to K_{IC} are considerably better for the underaged specimens compared to the overaged specimens. Carmen, et al.[11] in their study on the effect of purity on fracture toughness assumed that the energy absorbed may be considered as being divided into two parts. The first part consists of the surface energy and the second consists of the energy of plastic deformation. Assuming that the surface free energy term is approximately the same for similar materials then the differences in their values was due to the work of plastic deformation. Their assumption is borne out in the results of this study in that the percentage elongation values for the underaged specimens is consistently higher than those for the overaged specimens.

In Fig. 18, K_{IC} is plotted as a function of the strain hardening exponent, n. This shows a distinct trend of higher value of K_{IC} with greater strain hardening exponent, n. The K_{IC} value increases proportionately much greater than the increase in n. This plot substantiates the results of Carmen et al.[9] who attempted to explain the differences in K values for different test specimen rounds and sheets.

Of interest is the variation in the fracture mode as shown in Figs. 19(a) and (b). There is no change in mode due to specimen size and generally some variation in the profile due to the heat treatment. Underaged specimens fractured generally in a 0.25% or greater square mode while those overaged fractured in a full slant mode. Fully hardened specimens generally fractured in a V-slant mode.

In an effort to gain some insight into the behavior discussed, a metallographic examination was made of the alloy in the precipitation hardened condition and also in the underaged and overaged conditions. The structure in the T6 temper is shown in Fig. 20. The structures of underaged and overaged specimens from the test series 2 group are shown in Figs. 21 and 22. Studies of these figures reveal the alloy to have the same basic structure as evidenced by the elongated grains and precipitates. The T6 structure shows a dispersion of precipitated $MgZn_2$ phase and a very fine precipitate at the grain boundaries. The underaged structure shows very little precipitated $MgZn_2$ phase indicating that precipitation has only begun to take place while in the overaged structure, the precipitated particles have agglomerated and are more widely dispersed as shown in Fig. 22.

VII. SUMMARY AND CONCLUSIONS

The effects of overaging and underaging high strength 7075-T6 aluminum alloy to predetermined stress levels on the plane-strain fracture toughness has been investigated. The K_{IC}, K_{IC}/σ_{YS} and external energy absorbed to K_{IC} were determined as functions of the yield strength. K_{IC} was also determined as a function of the strain hardening exponent, n, and of the external energy absorbed to K_{IC}.

The plane-strain fracture toughness values were determined using the "pop-in" technique employing the single edge notch specimens of large and small sizes.

Due to the susceptibility of high strength 7075-T6 to stress corrosion in the underaged condition, future work on this topic will include determination of methods for effective straining without inhibiting the fracture toughness properties. The effect of straining following an underaging heat treatment (test series 2) resulted in an increase in plane strain fracture toughness from 38 ksi-$\sqrt{\text{in}}$ for the fully precipitation hardened condition to 48 ksi-$\sqrt{\text{in}}$.

Also, as accentuated by the size effects in Fig. 17, showing the external energy absorbed to K_{IC} plotted as a function of yield strength, there is the need for a stress analysis for the two specimen types that would include varying loading conditions. Work of this nature is to be continued.

From the results of this research the following may be concluded:

1. Overaging and underaging has the direct effect of increasing the plane-strain fracture toughness with a corresponding minimal loss

in the yield strength. The K_{IC} was increased from 38 ksi-$\sqrt{in}$ to 65 ksi $\sqrt{in}$ with an accompanying decrease in yield strength from 77 ksi to 66 ksi for the underaged specimens (test series 1). The K_{IC} was also increased from 38 ksi-$\sqrt{in}$ to 48 ksi-$\sqrt{in}$ for the overaged specimens (test series 1) with an accompanying decrease in yield strength from 77 ksi to 65 ksi.

2. The effect of underaging on the plane-strain fracture toughness is more pronounced than the effect of overaging and results in a better combination of strength and toughness.

3. The plane-strain fracture toughness of high strength 7075 always decreases with increasing yield strength in both the underaged and overaged conditions.

4. The work required to cause crack propagation is increased considerably by underaging and to a lesser degree by overaging with a corresponding minimal drop in the yield strength.

5. Direct correlation is obtained between measured tensile elongation and the value of external energy absorbed to K_{IC}.

6. A distinct trend of increasing values of plane-strain fracture toughness with increasing strain hardening exponent, n was observed.

7. The "pop-in" technique for measuring the plane-strain fracture toughness used in this research gives essentially the same values with the large and small size single edge notch specimens.

ACKNOWLEDGEMENTS

The author wishes to thank Professor E. R. Parker and Dr. D. Merz for their guidance, support and encouragement during the course of this investigation.

This work was performed under the auspices of the Unites States Atomic Energy Commission through the Inorganic Materials Research Division of the Lawrence Radiation Laboratory.

REFERENCES

1. R. W. Boyle, A. M. Sullivan and J. M. Krafft, Welding Journal, Research Supplement, 41 (9), 428-S (Sept. 1962).

2. D. M. Fisher, R. T. Bubsey and J. E. Srawley, Technical Note D-3724, NASA (Nov. 1966).

3. J. E. Srawley and W. F. Brown, Jr., NASA Tech. Memo., TM-X-52030.

4. A. M. Sullivan, Materials Research and Standards, 4, 20 (1964).

5. B. Gross, J. E. Srawley and W. F. Brown, Jr., Technical Note D-2395-NASA (August 1964).

6. J. E. Srawley and W. F. Brown, Jr., Fracture Toughness Testing and Its Application, ASTM STP No. 410 (ASTM, 1966), p. 12.

7. J. E. Srawley and W. F. Brown, Jr., Fracture Toughness Testing and Its Application, ASTM STP No. 381 (ASTM, 1965), p. 133.

8. W. A. Anderson, Precipitation from Solid Solution (ASM, 1959), p. 150-207.

9. C. M. Carman, D. F. Armiento and H. Markus, Trans. ASME 87, Series D, No. 4, December 1965.

10. J. E. Campbell, Defense Materials Information Center, DMIC Report 207, August 1964.

11. C. M. Carman, D. F. Armiento and H. Markus, Proceedings of the First International Conference on Fracture, Sendai, Japan, Vol. 2, p. 995, Sept. 1965. T. Yokobori, T. Kawasorki and J. L. Swedlow, Editors (The Japanese Society for Strength and Fracture of Materials, 1965).

12. G. E. Dieter Jr., Mechanical Metallurgy, (McGraw-Hill Book Company, New York, 1961), p. 198.

Table I. Test series 1. Engineering tensile and fracture properties of 7075-T6 aluminum alloy fully precipitation hardened

Type and Treatment	Tensile				Fracture								
	Elong. %	σ_{YS} ksi	σ_{UTS} ksi	σ_{FS} ksi	K_{IC} ksi-$\sqrt{in}$	σ ksi	K_C ksi-$\sqrt{in}$	σ ksi	External energy absorbed to K_{IC} in-lb/in^2	External energy absorbed to K_C in-lb/in^2	$\frac{K_{IC}}{\sigma_{YS}}$	Strain Hardening Exponent n	Strength Coefficient k ksi
Large size precipitation hardened (a)	14.1	77.3	83.7	81.0	38	16.4	46	19.6	497	760	0.492	0.054	80.3
Small size precipitation hardened (b)	14.5	77.4	83.8	82.0	41	16.0	41	16.0	375	-	0.530	0.086	75.7

(a) See Figs.2(a) and 3(a).

(b) See Figs.2(b) and 3(b).

Table II. Test series 1. Engineering tensile and fracture properties of large size 7075-T6 specimens overaged to an average yield strength of 65,000 psi

	Tensile				Fracture								
Type and Treatment	Elong. %	σ_{YS} ksi	σ_{UTS} ksi	σ_{FS} ksi	K_{IC} ksi-$\sqrt{in}$	σ ksi	K_C ksi-$\sqrt{in}$	σ ksi	External energy absorbed to K_{IC} in-lb/in^2	K_C in-lb/in^2	$\frac{K_{IC}}{\sigma_{YS}}$	Strain Hardening Exponent n	Strength Coefficient k ksi
Overaged at 325°F for 11.5 hours	13	69.4	77.6	72.8	44	18.7	50	21.7	680	1175	0.635	0.076	72.3
Overaged at 350°F for 6.5 hours	13	63.6	72.8	66.1	47	19.9	55	23.6	810	1250	0.74	0.088	66.8
Overaged at 375°F for 100 mins.	12.5	70.5	78.3	73.0	45	18.9	51	22.7	692	1078	0.637	0.08	73.0
Overaged at 400°F for 42 mins.	12.5	66.7	75.1	69.7	46	19.6	55	23.6	764	1205	0.69	0.090	68.7
Overaged at 425°F for 12 mins.	11	63.5	72.7	67.0	46	19.6	56	23.9	767	1340	0.725	0.078	68.1

Table III. Test series 1. Engineering tensile and fracture properties of large size 7075-T6 specimens underaged to an average yield stress of 66,000 psi

	Tensile				Fracture								
Type and Treatment	Elong. %	σ_{YS} ksi	σ_{UTS} ksi	σ_{FS} ksi	K_{IC} ksi-$\sqrt{in}$	σ ksi	K_C ksi-$\sqrt{in}$	σ ksi	External energy absorbed to K_{IC} in-lb/in^2	External energy absorbed to K_C in-lb/in^2	$\frac{K_{IC}}{\sigma_{YS}}$	Strain Hardening Exponent n	Strength Coefficient k ksi
Resolution heat treated at 870°F for 30 mins. and precipitation hardened at 250°F for 28 hours	14	73.9	82.9	82.9	49	20.6	56	23.9	825	1220	0.664	0.076	74.9
Underaged at 250°F for 5 hours (a)	15.5	66.5	80.8	80.8	61	26.0	65	27.6	1525	1930	0.916	0.107	70.2
Underaged at 275°F for 3 hours (a)	15.5	67.0	80.0	80.0	61	26.0	64	27.2	1509	1760	0.910	0.107	69.7
Underaged at 300°F for 50 mins. (a)	16	63.5	77.6	77.6	65	27.6	68	28.8	2015	2430	1.023	0.106	67.3

(a) Specimens were solution heat treated at 870°F for 0.5 hours prior to artificial aging.

Table IV. Test series 2. Engineering tensile and fracture properties of small size 7075-T6 specimens overaged to an average yield stress of 70,000 psi

Type and Treatment	Tensile				Fracture			External energy absorbed to K_{IC} ksi $\sqrt{in}$	$\frac{K_{IC}}{\sigma_{YS}}$	Strain hardening exponent n	Strength coefficient k ksi
	Elong. %	σ_{YS} ksi	σ_{UTS} ksi	σ_{FS} ksi	K_{IC} ksi$\sqrt{in}$	Stress at K_{IC} σ ksi	Fracture Stress σ ksi				
Overaged at 300°F for 12 hours	13.5	73.0	81.4	74.6	42	16.6	16.6	450	0.575	0.125	68.1
Overaged at 325°F for 9 hours	15	69.5	78.6	68.2	47	18.3	18.3	505	0.675	0.123	70.6
Overaged at 350°F for 2.5 hours	15	68.0	77.0	67.4	47	18.2	18.2	513	0.692	0.124	64.0
Overaged at 375°F for 36 mins.	14	69.6	78.6	68.3	44	17.2	17.2	460	0.631	0.113	67.8
Overaged at 400°F for 12 mins.	13	68.6	77.6	68.6	45	17.6	17.6	463	0.655	0.115	66.5

Table V. Test Series 2. Engineering tensile and fracture properties of small size 7075-T6 specimens underaged to an average yield stress of 70,000 psi.

Type and Treatment	Tensile				Fracture						
	Elong. %	σ_{YS} ksi	σ_{UTS} ksi	σ_{FS} ksi	K_{IC} ksi$\sqrt{in}$	Stress at K_{IC} σ ksi	Fracture Stress σ ksi	External energy absorbed to K_{IC} ksi $\sqrt{in}$	$\frac{K_{IC}}{\sigma_{YS}}$	Strain hardening exponent n	Strength coefficient k ksi
Resolution heat treated at 870°F for 0.5 hrs and precipitation hardened at 250°F for 28 hrs.	13	77.0	86.0	83.0	55	21.6	21.6	705	0.786	0.101	74.5
Underaged[a] at 250°F for 10 hrs.	16.5	69.0	83.0	78.7	55	21.6	21.6	733	0.800	0.141	65.6
Underaged[a] at 275°F for 7 hrs.	16	72.2	82.0	76.4	54	21.0	21.0	675	0.750	0.113	69.5
Underaged[a] at 300°F for 3 hrs.	14.5	70.0	80.0	75.5	54	21.2	21.2	707	0.700	0.121	73.8

(a) Specimens were solution heat treated at 870°F for 0.5 hrs. prior to artificial aging.

Table VI. Test Series 2. Engineering tensile and fracture properties of small size 7075-T6 specimens underaged (strained 1% and reaged 15% of prior heat treatment) to an average yield stress of 70,000 psi.

Type and Treatment	Tensile				Fracture						
	Elong. %	σ_{YS} ksi	σ_{UTS} ksi	σ_{FS} ksi	K_{IC} ksi$\sqrt{in}$	Stress at K_{IC} σ ksi	Fracture Stress σ ksi	External energy absorbed to K_{IC} ksi $\sqrt{in}$	$\frac{K_{IC}}{\sigma_{YS}}$	Strain hardening exponent n	Strength coefficient k ksi
Reprecipitation hardened 250°F for 28 hrs- Strained and reaged at 250°F for 4.2 hrs. (a)	13	75.0	85.5	82.4	38	15.0	15.4	360	0.507	0.117	72.4
underaged 250 °F for 10 hrs, strained (b) and reaged at 250°F 1.5 hrs. (a)	13	73.0	84.0	82.0	43	16.7	16.7	433	0.590	0.128	69.3
Underaged at 275°F for 7 hrs, strained and reaged at 275°F for 63 mins. (a) (b)	13	71.0	81.6	77.0	44	17.2	17.2	460	0.620	0.120	67.1

Table VI. (Continued)

Type and Treatment	Tensile				Fracture			External energy absorbed to K_{IC} ksi $\sqrt{in}$	$\frac{K_{IC}}{\sigma_{YS}}$	Strain hardening exponent n	Strength coefficient k ksi
	Elong. %	σ_{YS} ksi	σ_{UTS} ksi	σ_{FS} ksi	K_{IC} ksi$\sqrt{in}$	Stress at K_{IC} σ ksi	Fracture Stress σ ksi				
(a) Underaged at 300°F -3 hrs, strained (b) and reaged at 300°F -27 min	13.5	69.5	80.0	73.3	48	18.6	18.6	546	0.690	0.121	71.6
(a) Underaged at 300°F -3 hrs, strained (b) and reaged at 300°F-27 min.	—	—	—	—	48	18.8	18.8	584	—	—	—

(a) Specimens were solution heat treated at 870°F for 0.5 hrs prior to artificial aging.

(b) Specimens were strained 1% of original thickness.

Table VII. Test Series 3. Engineering tensile and fracture properties of small size 7075-T6 specimens overaged to an average yield stress of 63,000 psi.

Type and Treatment	Tensile				Fracture			External energy absorbed to K_{IC} ksi $\sqrt{in}$	$\frac{K_{IC}}{\sigma_{YS}}$	Strain hardening exponent n	Strength coefficient k ksi
	Elong. %	σ_{YS} ksi	σ_{UTS} ksi	σ_{FS} ksi	K_{IC} ksi$\sqrt{in}$	Stress at K_{IC} σ ksi	Fracture Stress σ ksi				
Overaged at 325°F for 11.5 hrs.	14.5	68.8	77.4	67.9	47	18.1	18.1	506	0.684	0.123	64.7
Overaged at 350°F for 6.5 hrs.	15.5	64.7	74.0	62.6	48	18.5	18.5	555	0.730	0.134	60.5
Overaged at 375°F for 1.66 hrs.	16.5	62.8	73.0	61.5	49	19.0	19.0	640	0.780	0.130	60.0
Overaged at 400°F for 42 mins.	15.5	58.6	69.6	59.4	48	18.5	18.5	650	0.818	0.152	55.0
Overaged at 425°F for 12 mins.	15.5	59.6	70.5	60.4	47	18.4	18.4	600	0.790	0.144	56.0

Table VIII. Test Series 3. Engineering tensile and fracture properties of small size 7075-T6 specimens underaged to an average yield stress of 66,000 psi.

Type and Treatment	Tensile				Fracture						
	Elong. %	σ_{YS} ksi	σ_{UTS} ksi	σ_{FS} ksi	K_{IC} ksi$\sqrt{in}$	Stress at K_{IC} σ ksi	Fracture Stress σ ksi	External energy absorbed to K_{IC} ksi $\sqrt{in}$	$\frac{K_{IC}}{\sigma_{YS}}$	Strain hardening exponent n	Strength coefficient k ksi
Underaged at 250°F for 5 hrs. (a)	16.5	68.0	81.4	78.2	57	22.0	22.0	1035	0.839	0.128	66.0
Underaged at 275°F for 3 hrs. (a)	16.5	68.4	81.8	74.6	59	23.0	23.0	1220	0.863	0.129	65.0
Underaged at 300°F for 50 mins. (a)	16	67.0	77.7	73.5	56	21.6	21.6	965	0.836	0.145	61.0

(a) Specimens were solution heat treated at 870°F for 0.5 hrs. prior to artificial aging.

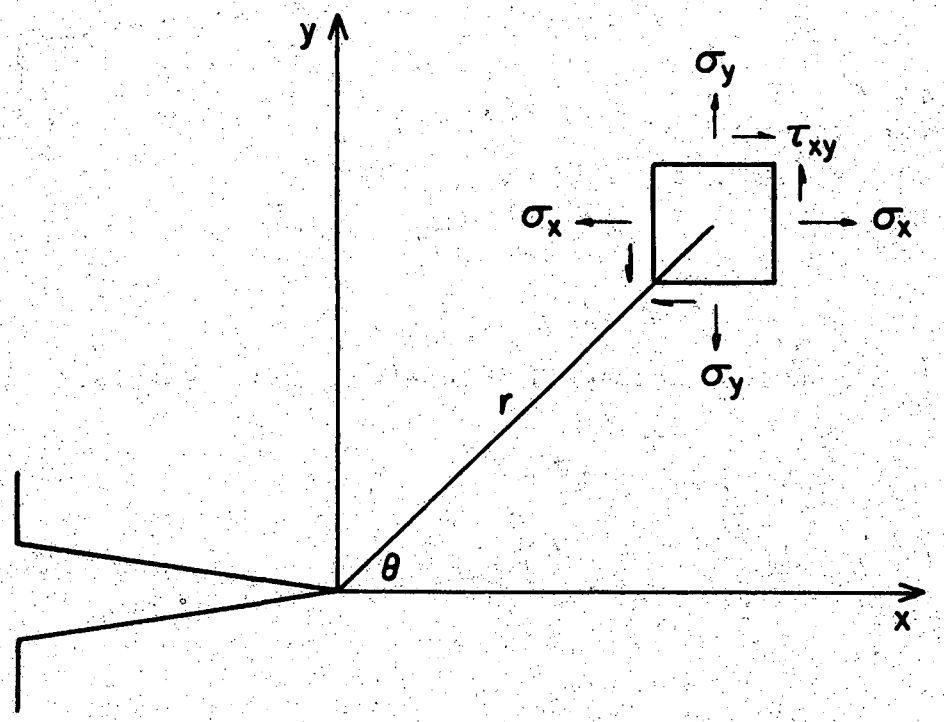

XBL 679-4967

Fig. 1. Stresses acting on element of material near the crack tip.

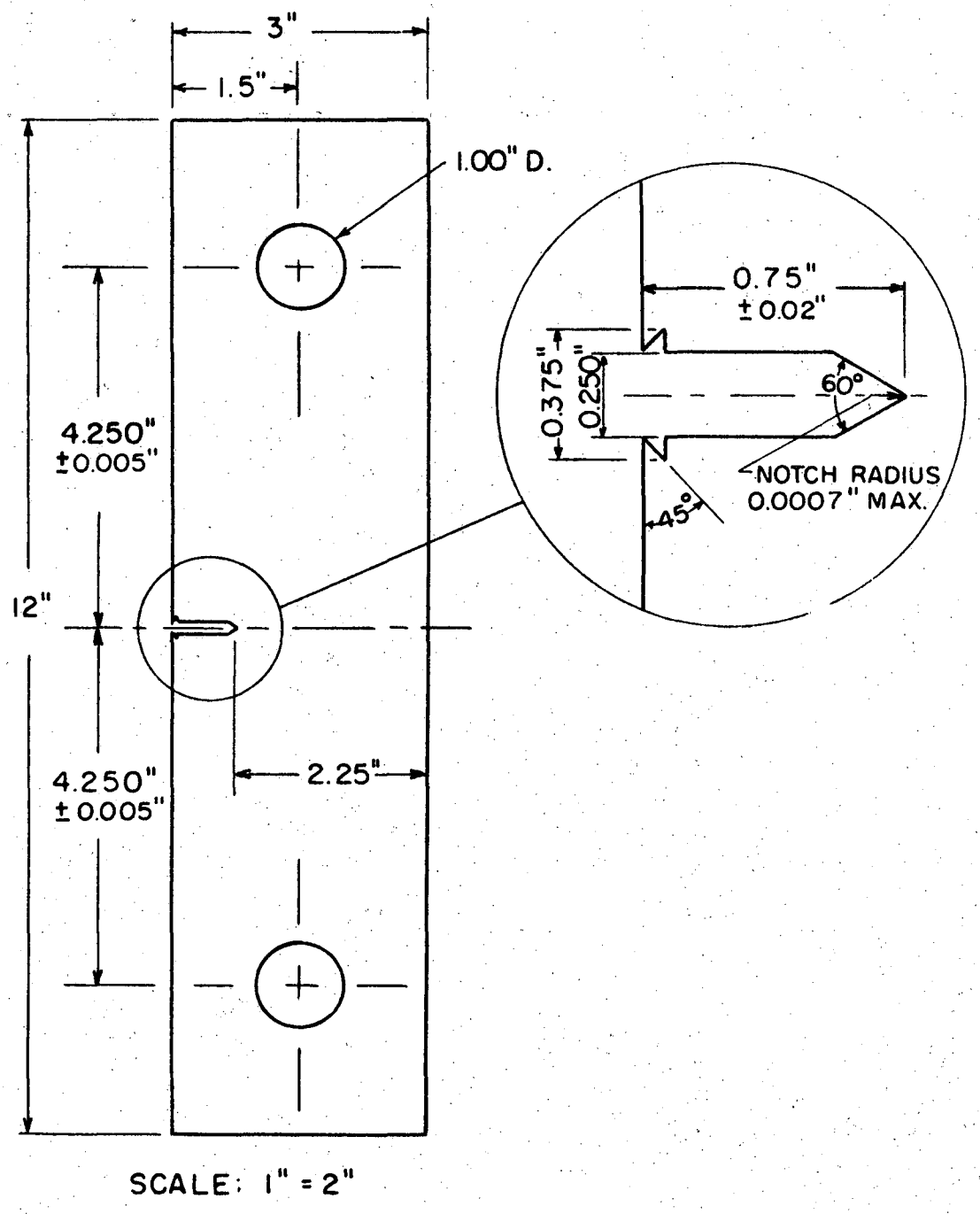

XBL 679-4969

Fig. 2. Fracture specimens used in the determination of mechanical properties in accordance with ASTM standards.
(a) Large type single edge notch specimen 12"×3"× 1/4" thick showing single edge notched details.

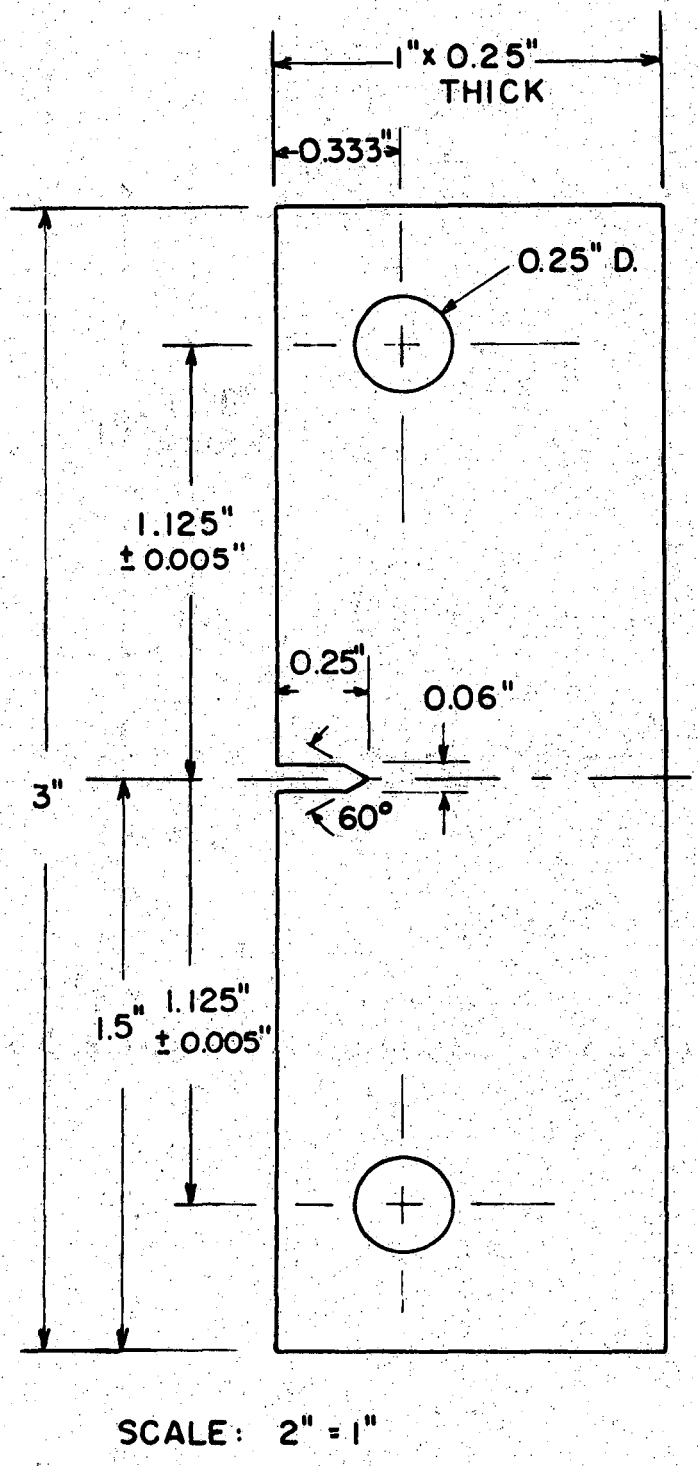

XBL 679-4970

Fig. 2(b). Small type single edge notched specimen 3"×1"×1/4" thick.

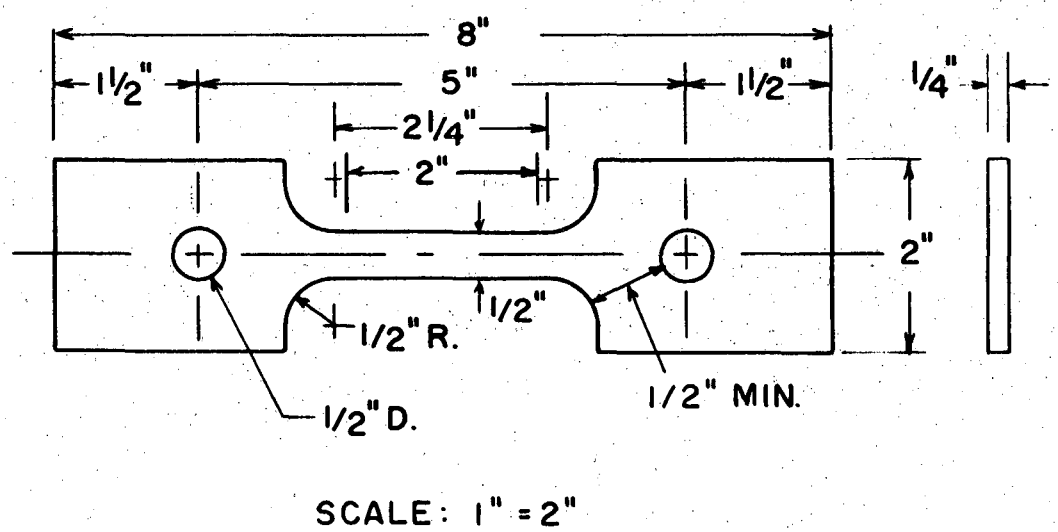

XBL 679-4972

Fig. 3. Tensile specimens used in the determination of mechanical properties in accordance with ASTM standards.
(a) Large gauge tensile specimen with a 2" gauge length and 0.250" thickness.

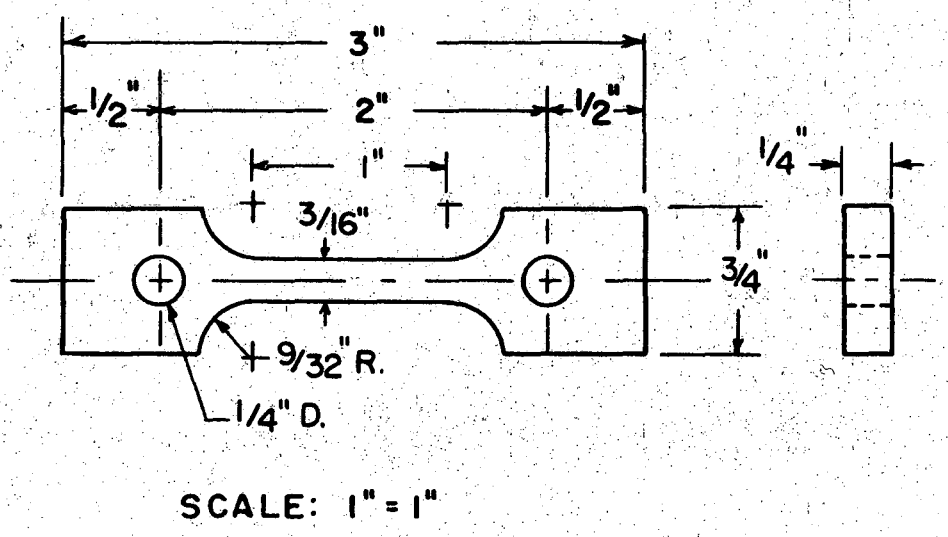

XBL 679-4968

Fig. 3(b). Short gauge tensile specimen with a 1" gauge length and 0.250" thickness.

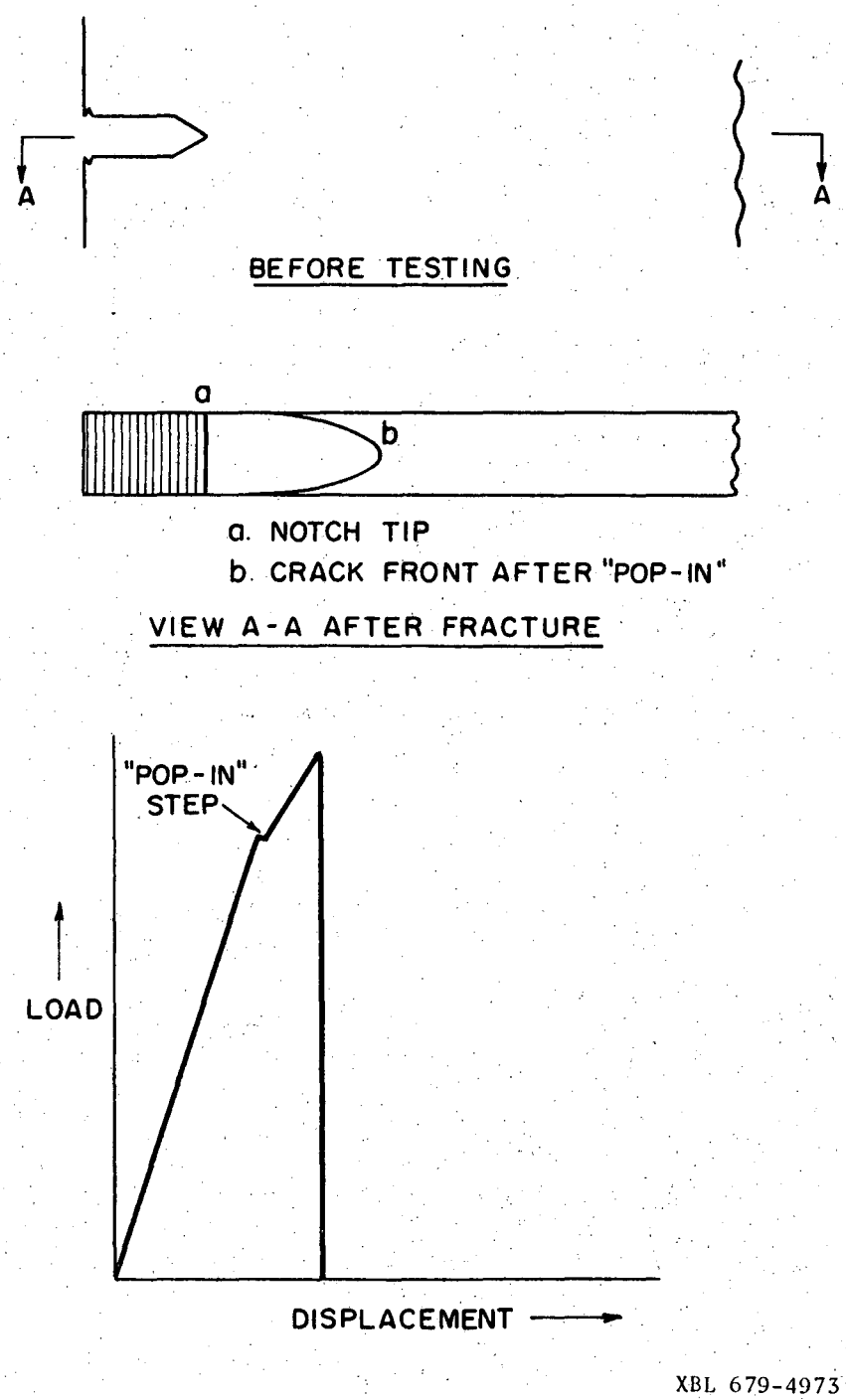

Fig. 4. Schematic load-displacement plot for tests of single edge notched specimens.

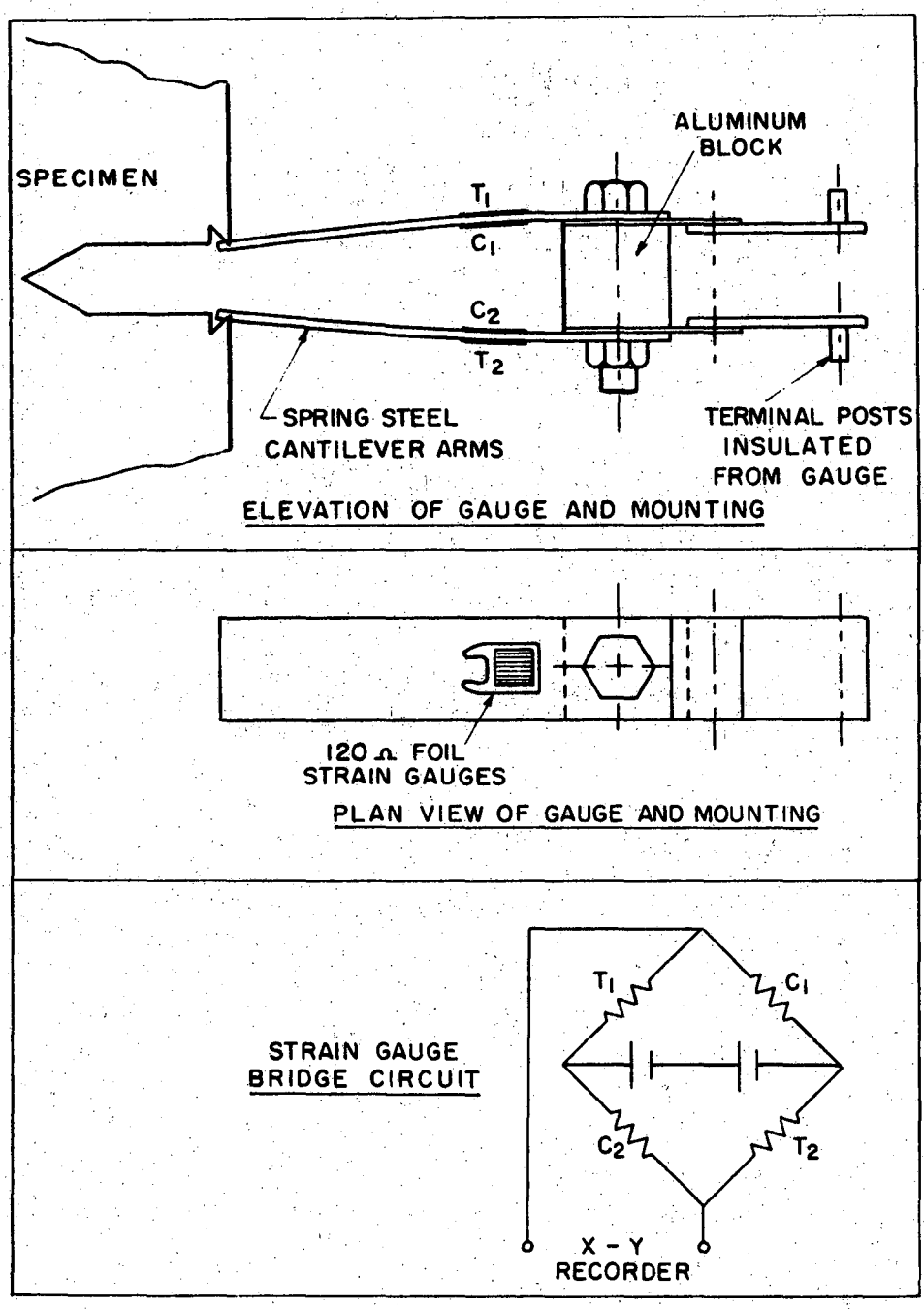

XBL 679-4971

Fig. 5. Double cantilever beam gauge and method of mounting on large single edge notched specimens for displacement measurement.

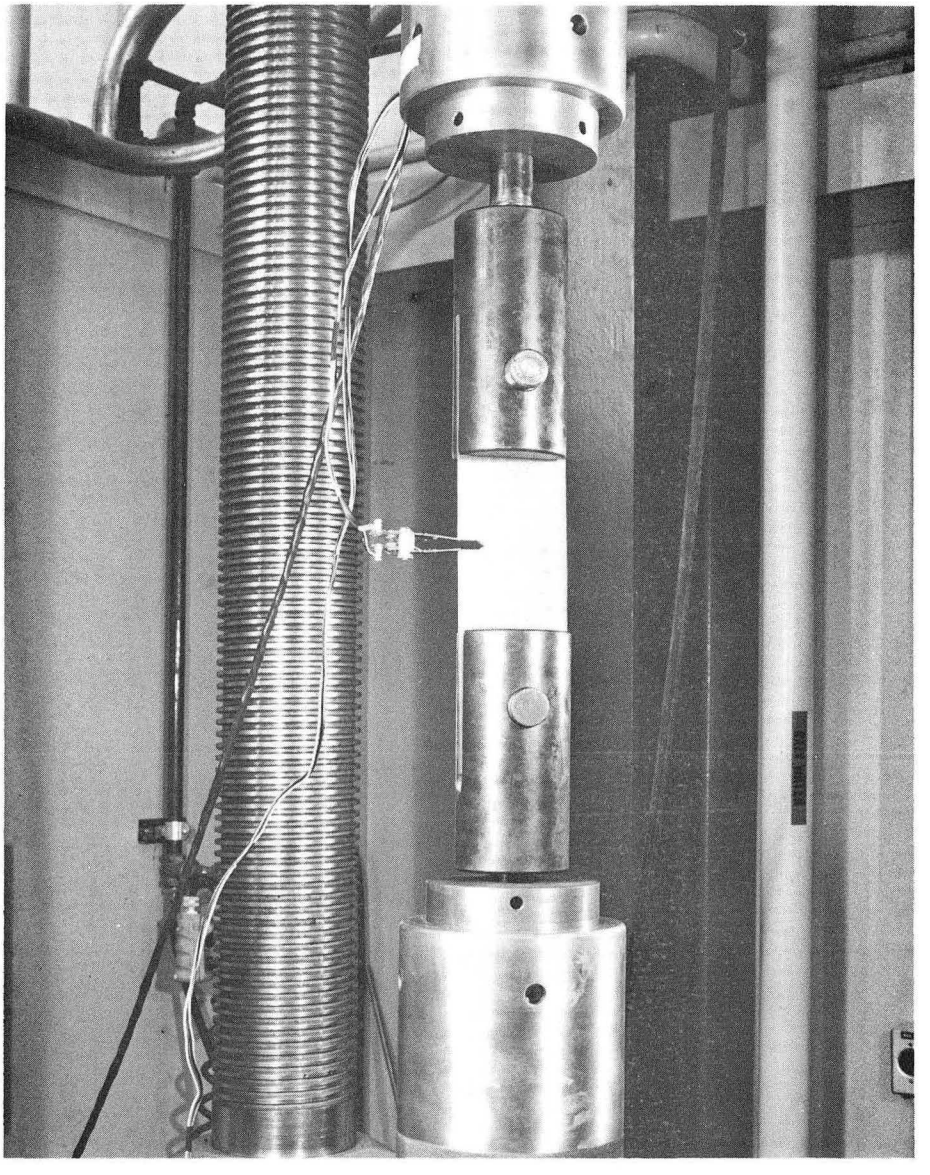

XBB 679-5262

Fig. 6. Large type single edge notch specimen with the compliance gauge in position mounted on the M. T. S. 300 kip testing machine.

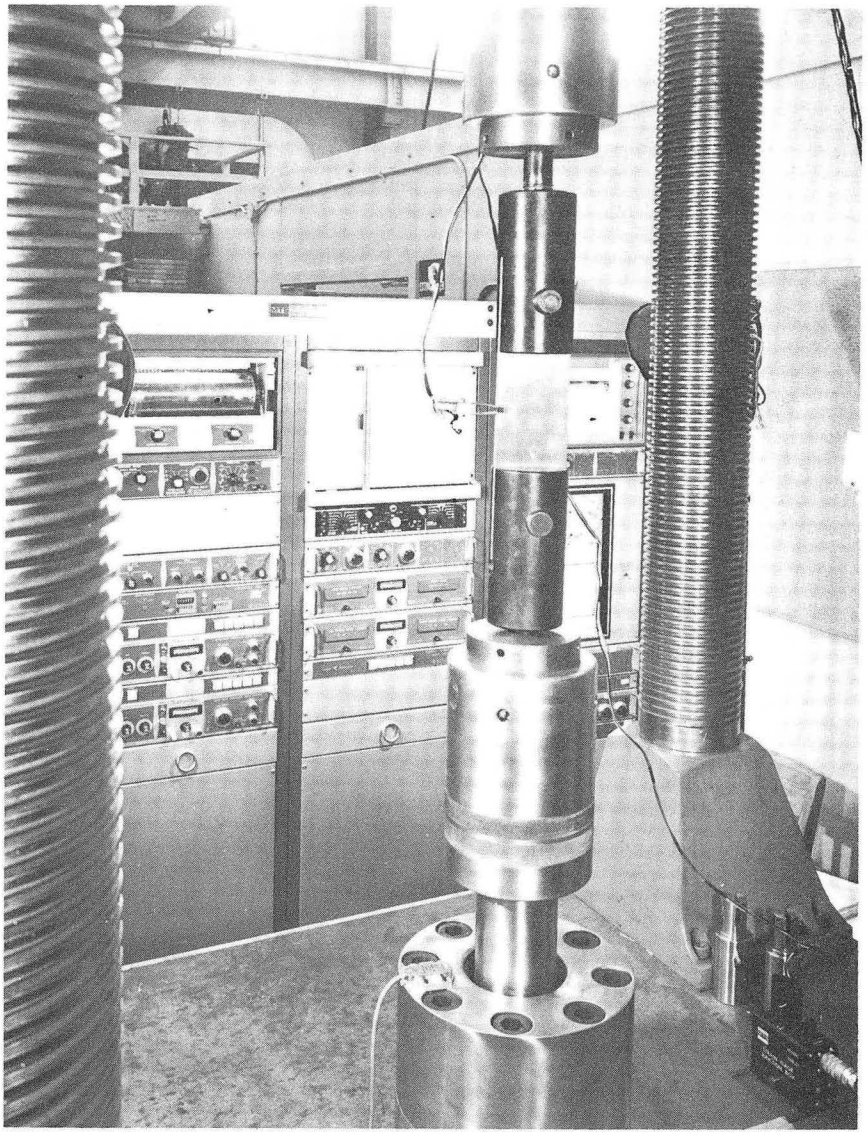

XBB 679-5264

Fig. 7. Experimental arrangement using the M. T. S. 300 kip testing machine.

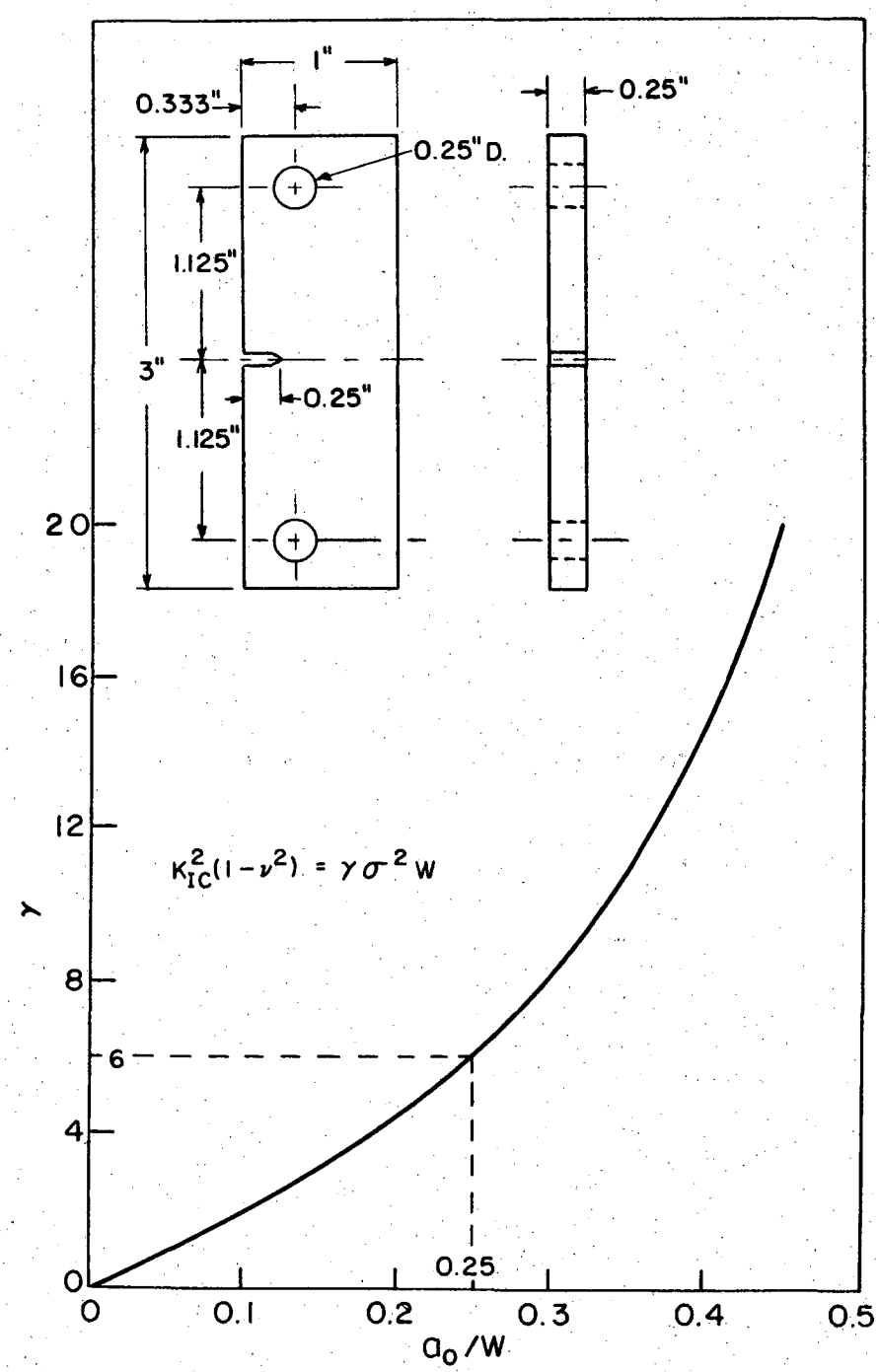

XBL 679-4977

Fig. 8. Calibration curve derived from compliance measurements[4] used in the evaluation of K_{IC} for large single edge notched specimens.

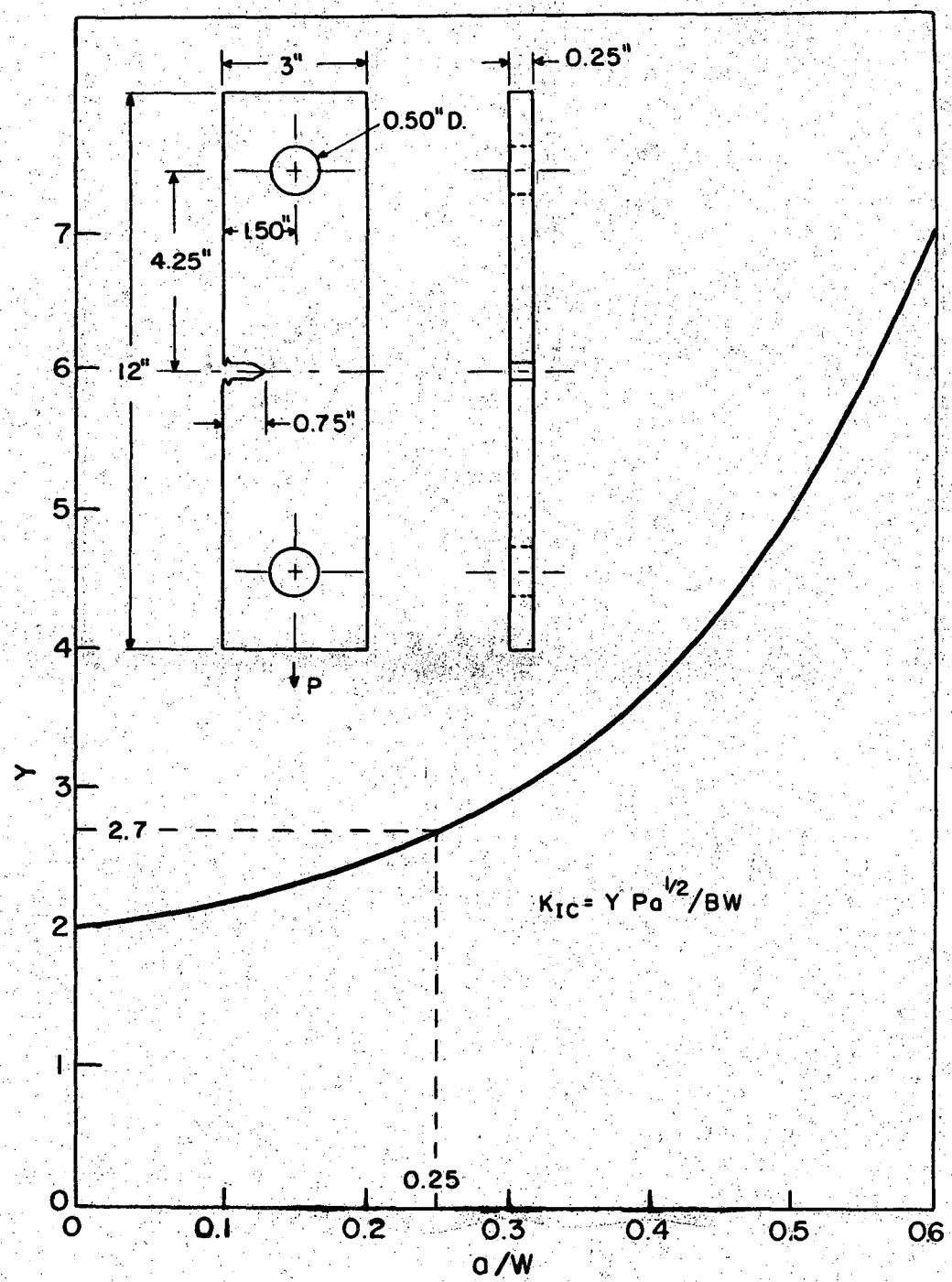

XBL 679-4976

Fig. 9. Calibration curve derived from the boundary collocation procedures[5] used in the evaluation of K_{IC} for small single edge notched specimens.

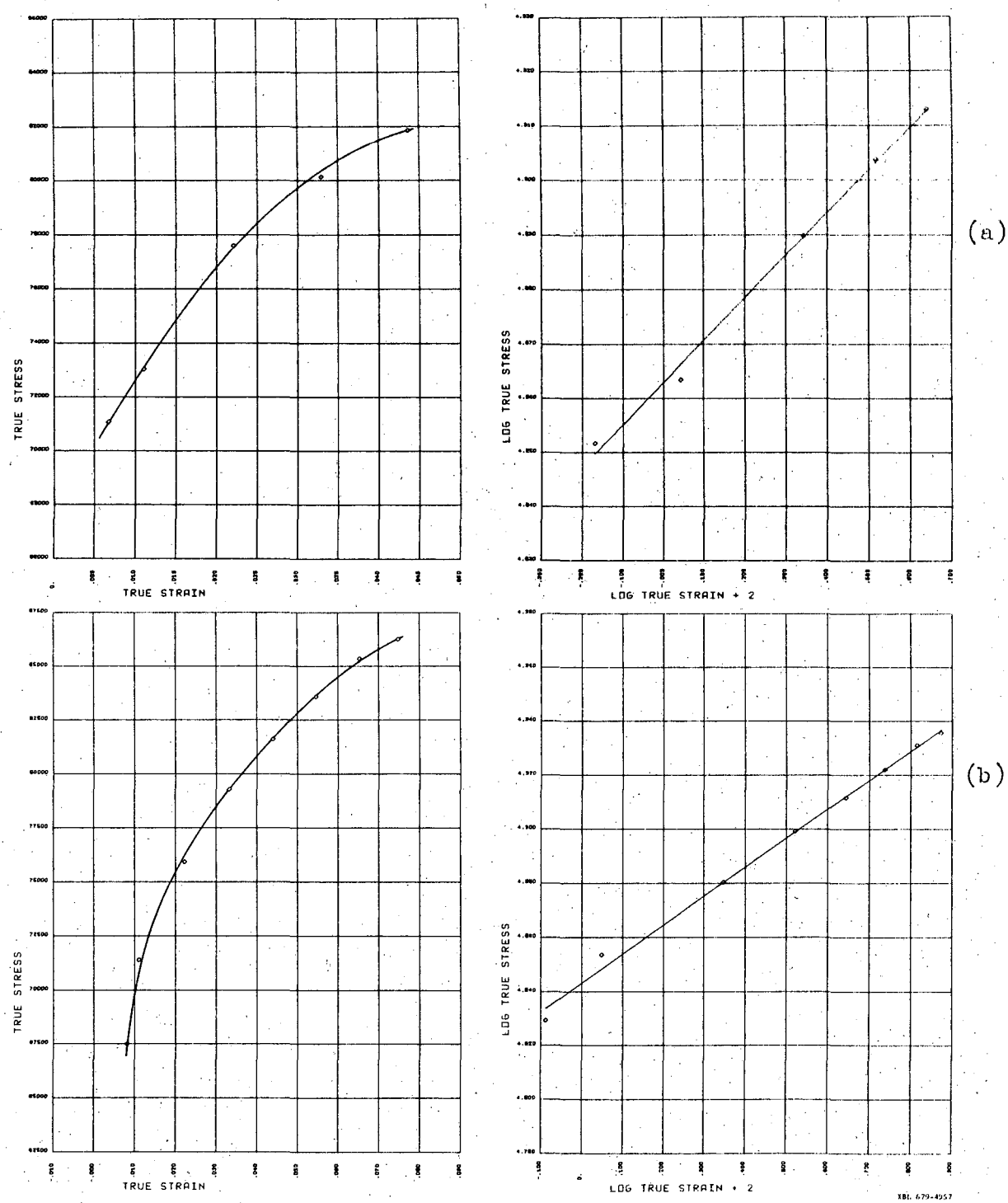

Fig. 10. Computer plots of true stress versus true strain and log true stress versus log true strain.
(a) 7075-T6 typically overaged from test series 1.
(b) 7075-T6 typically underaged from test series 1.

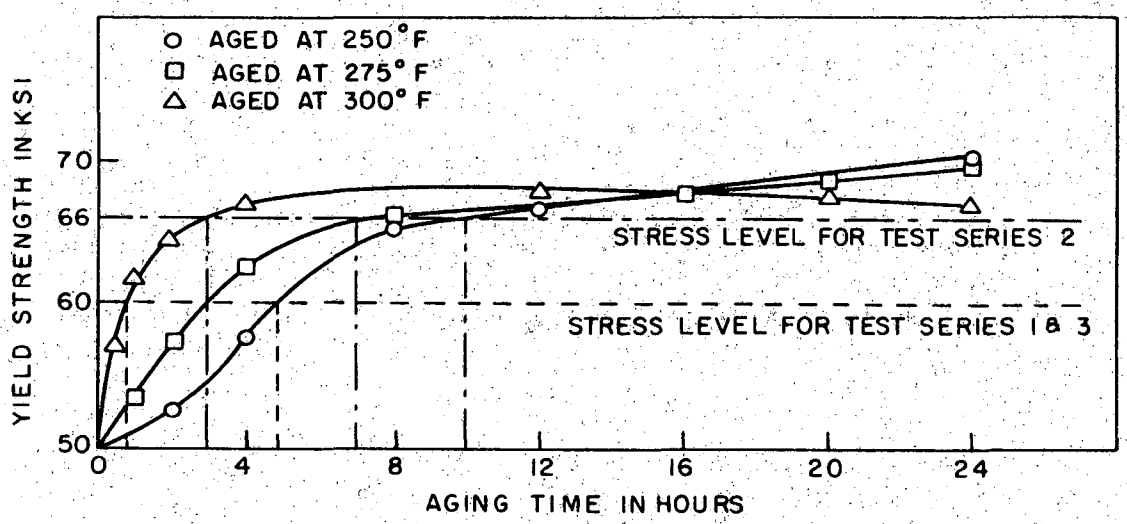

XBL 679-4975

Fig. 11. Artificial aging of 7075 sheet. (W. A. Anderson, Precipitation from Solid Solution, American Society for Metals, 1959, p. 182.) The stress levels selected for the overaging indicate the time and temperature treatments.

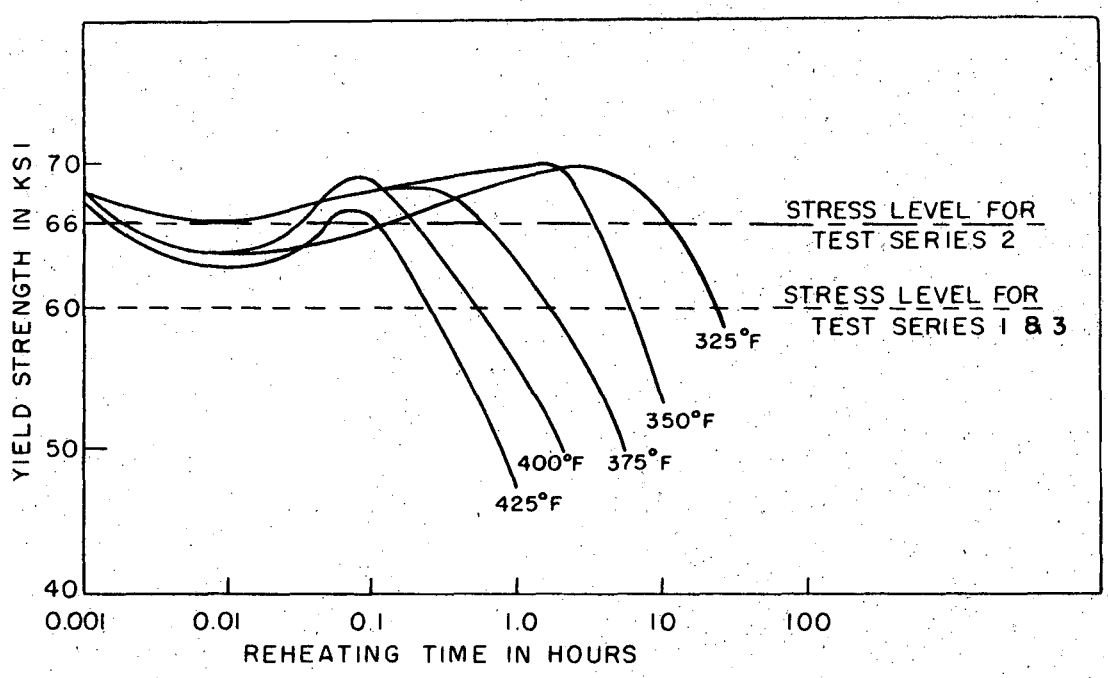

XBL 679-4974-A

Fig. 12. The effects of reheating time and temperature on the yield strength property of 7075 sheet. (W. A. Anderson, Precipitation from Solid Solution, American Society for Metals, 1959, p. 184.) The stress levels for the under-aging are shown.

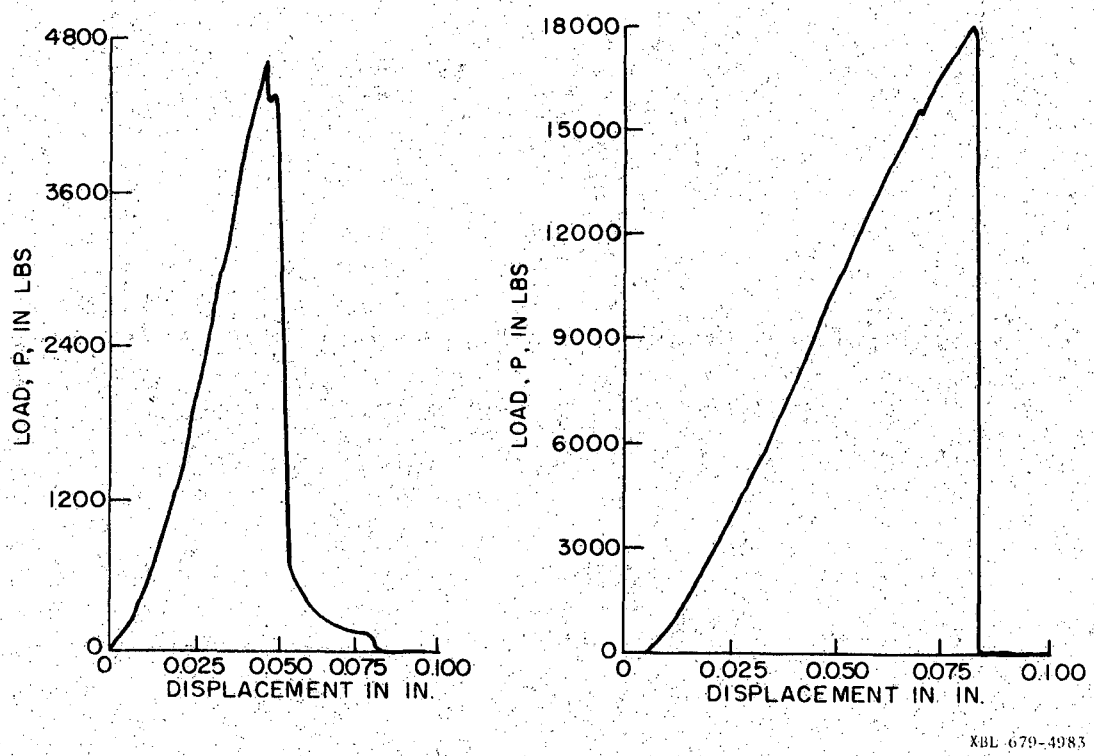

Fig. 13. Load-displacement curves for the two fracture specimen sizes.

(a) Curve for the small type single edge notched specimens shows the "pop-in" and fracture points as being coincident.

(b) Curve for the large type single edge notched specimen shows the "pop-in" before fracture.

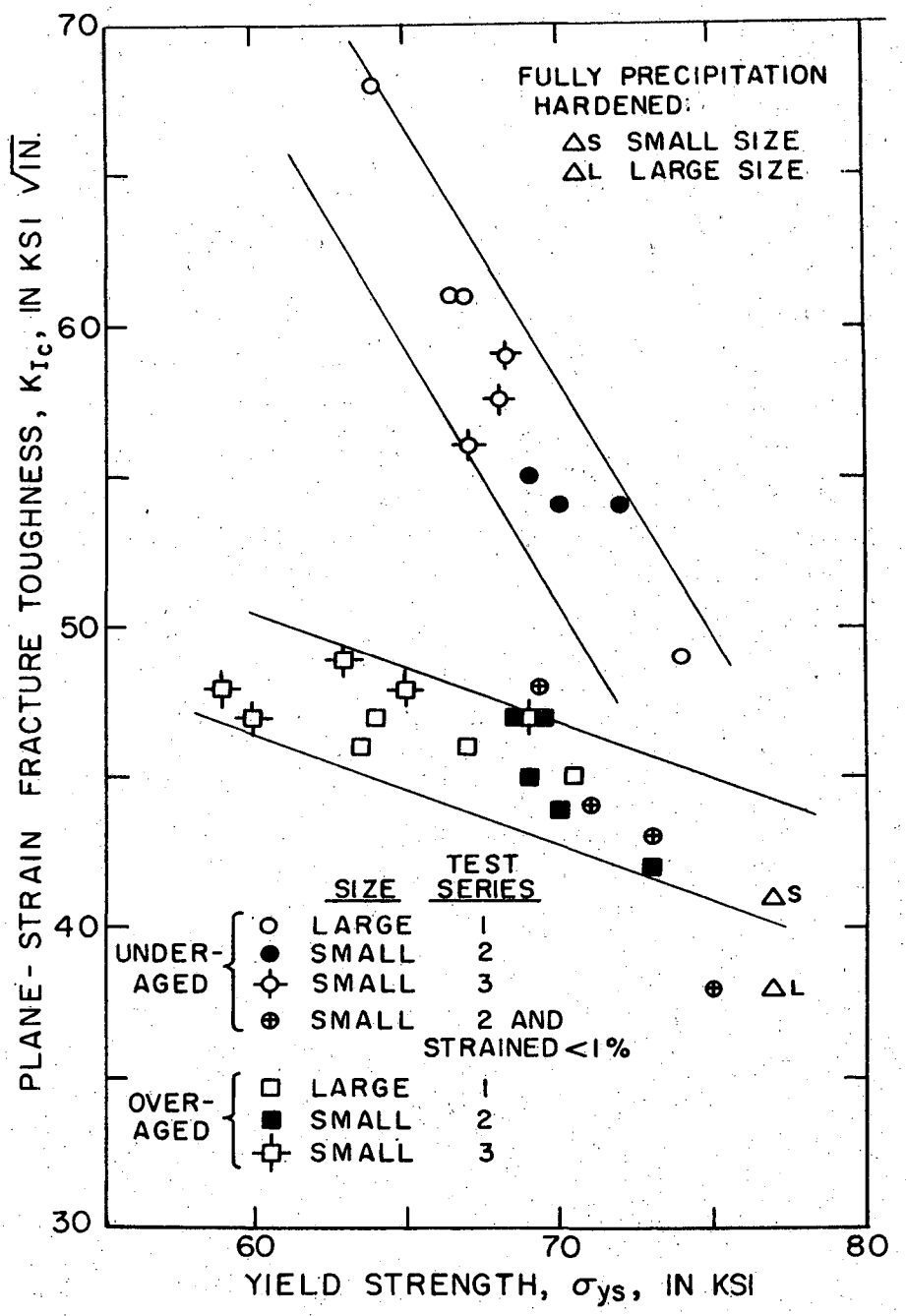

XBL 679-4978A

Fig. 14. The plane-strain fracture toughness values determined by "pop-in" method for high strength 7075-T6 for all specimens versus yield strength.

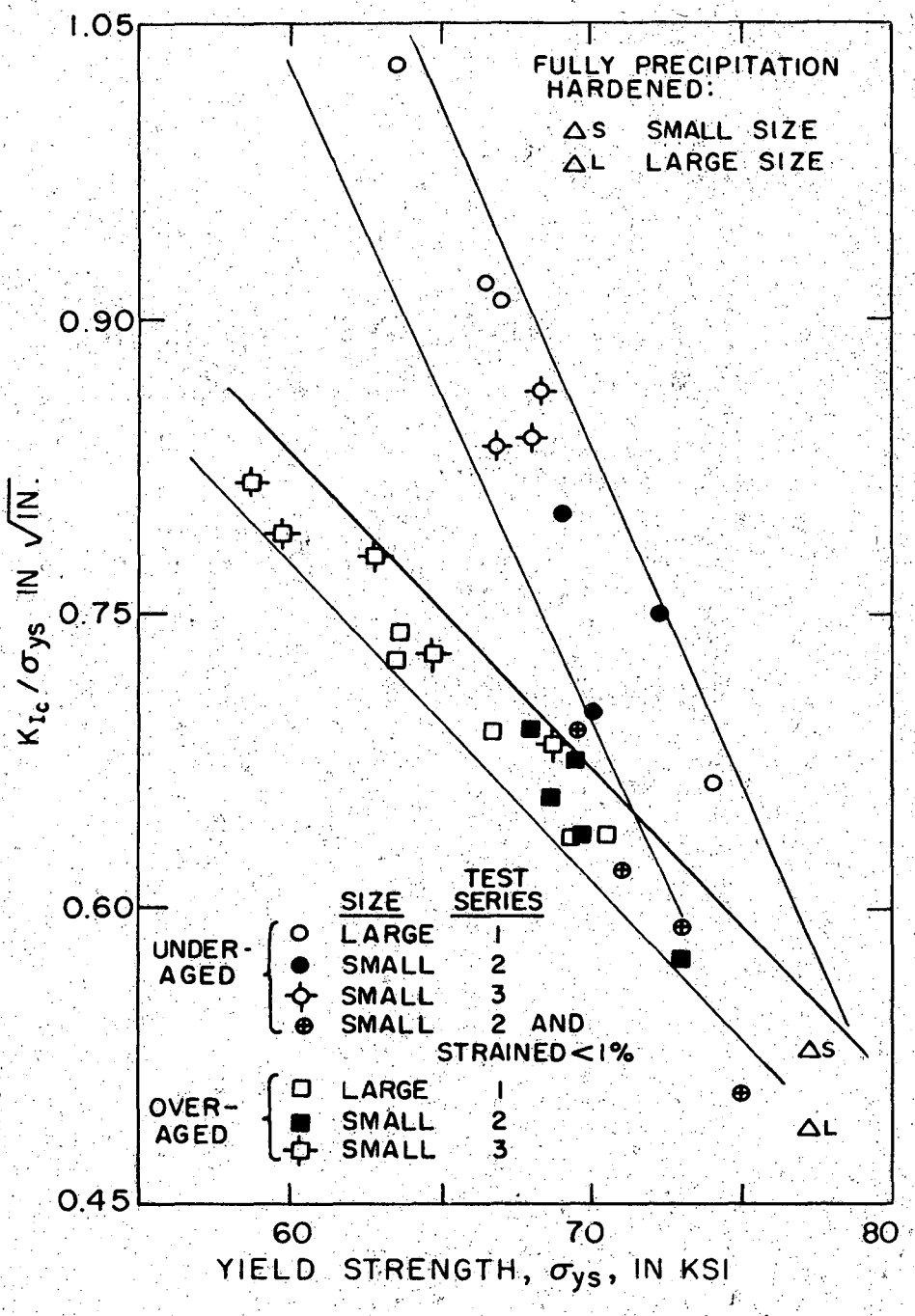

XBL 679-4980

Fig. 15. K_{IC}/σ_{YS} for high strength 7075-T6 for all specimens as a function of yield strength.

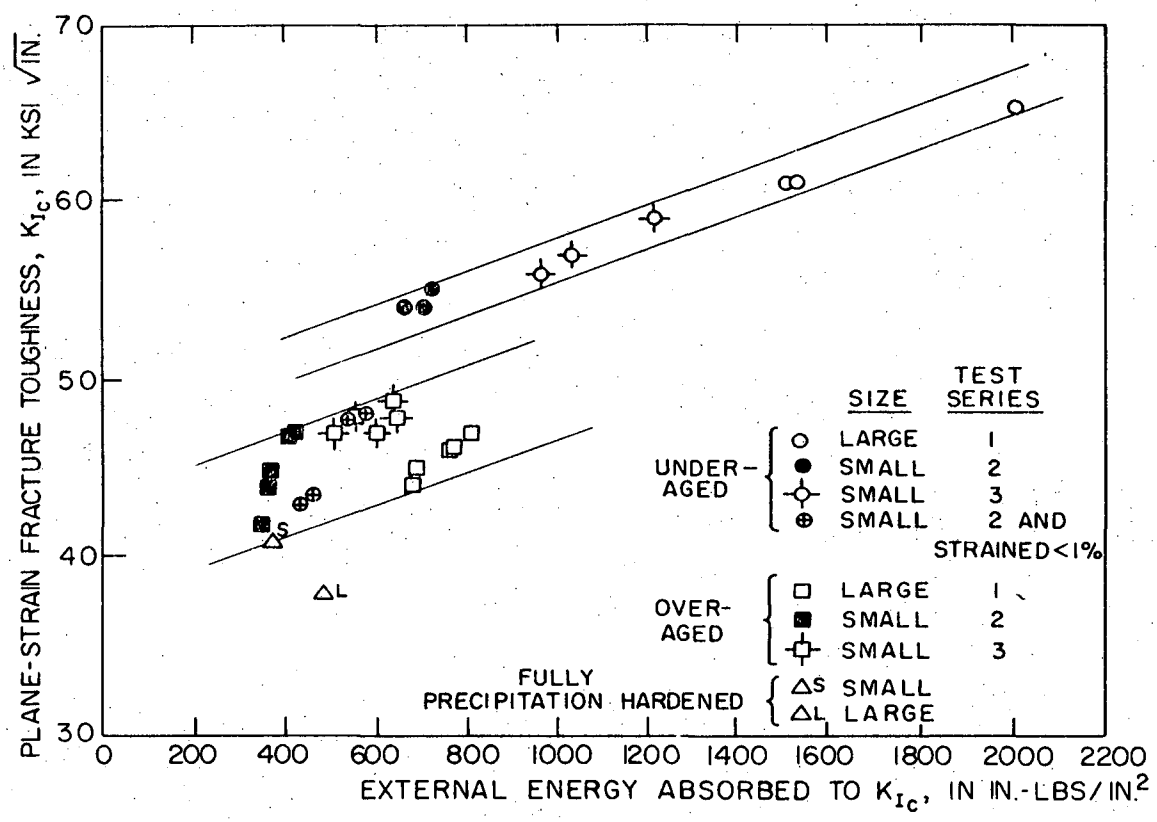

XBL 679-4982

Fig. 16. Plane-strain fracture toughness of high strength 7075-T6 for all specimens as a function of external energy absorbed to plane-strain fracture toughness.

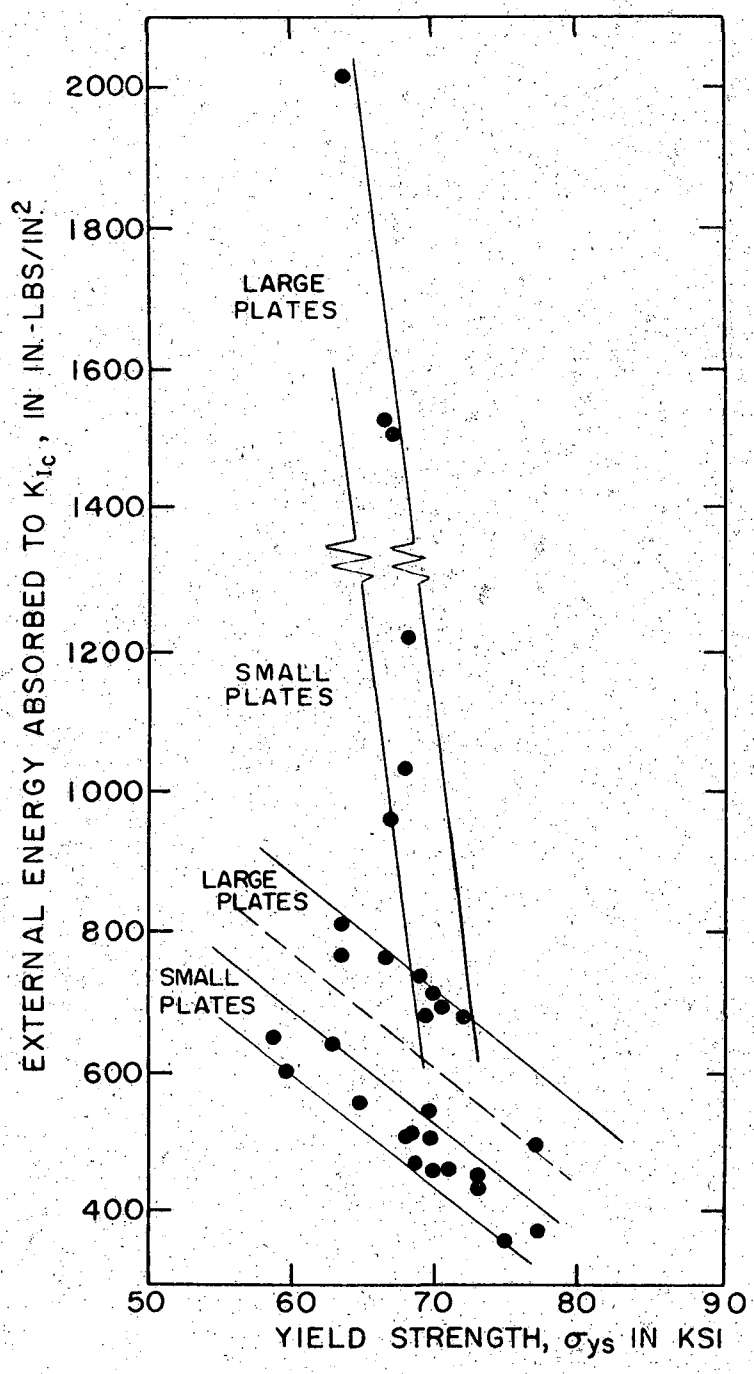

XBL 679-4981

Fig. 17. External energy absorbed to K_{IC} due to the loading conditions for high strength 7075-T6 for all specimens as a function of yield strength. Lower two bands are overaged and upper band is underaged.

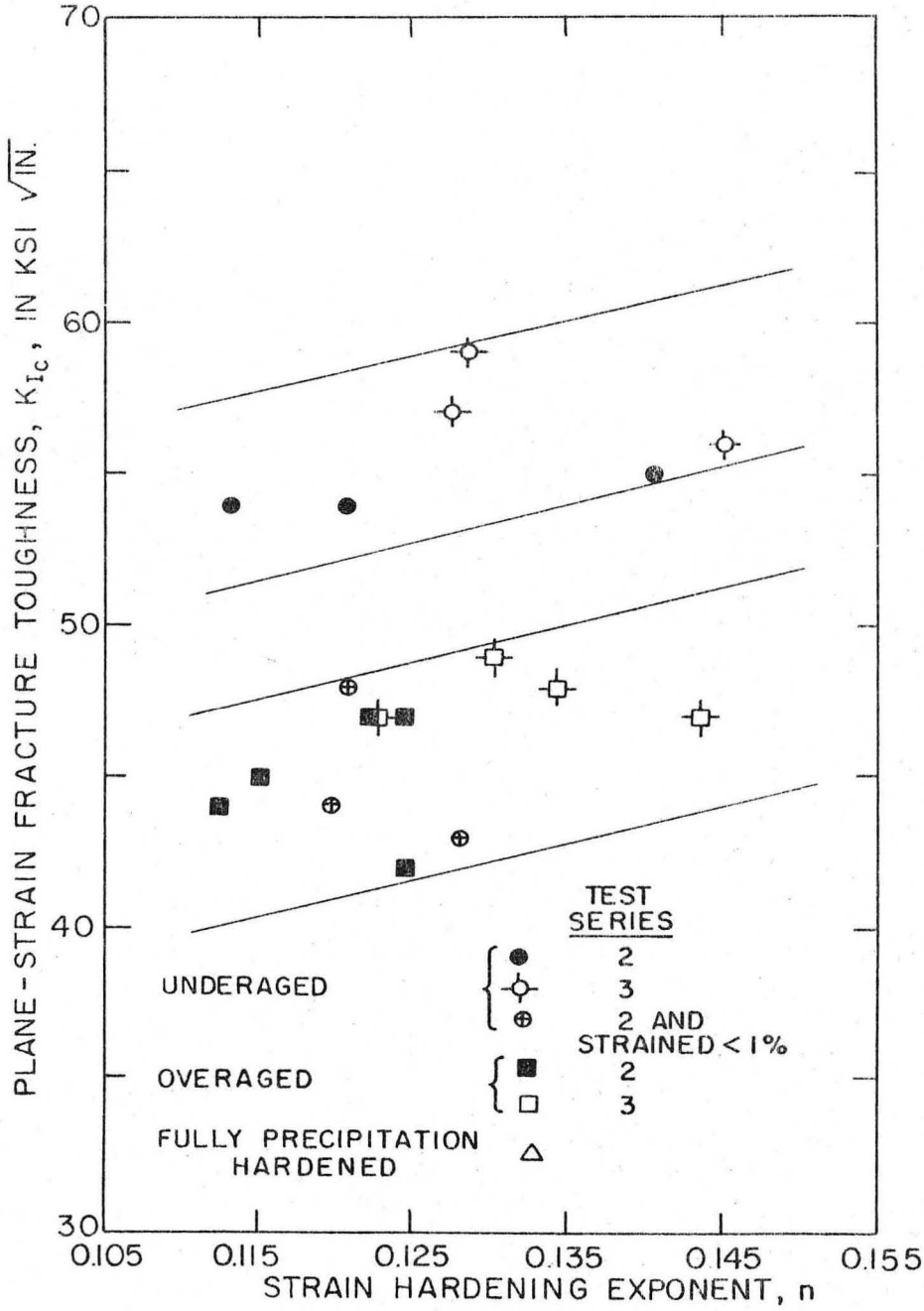

XBL 679-4979

Fig. 18. Plane-strain fracture toughness for high strength 7075-T6 for all specimens as a function of the strain hardening exponent.

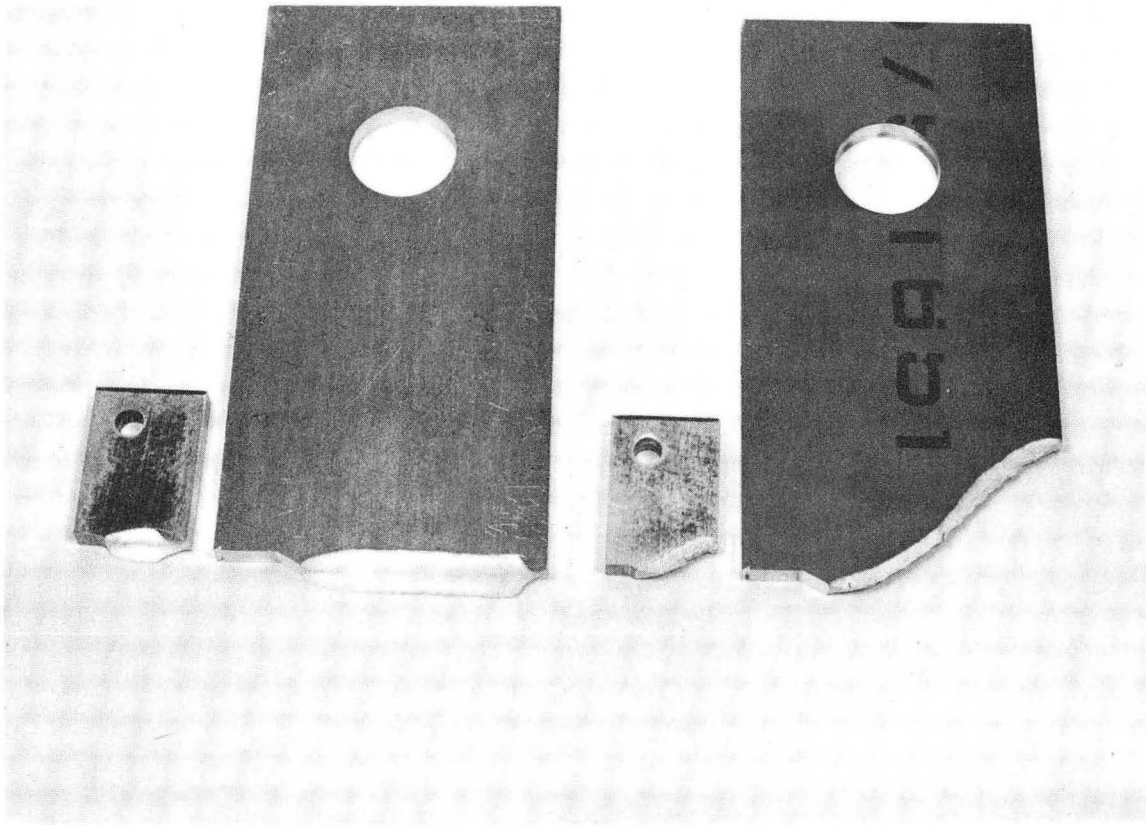

XBB 679-5506

(a) (b)

Fig. 19. Fracture modes of the two types of fracture specimens.
(a) Comparison of small and large types of single edge notched specimens underaged in test series 3.
(b) Comparison of small and large types of single edge notched specimens in the fully precipitation hardened condition.

63×

Keller's etch

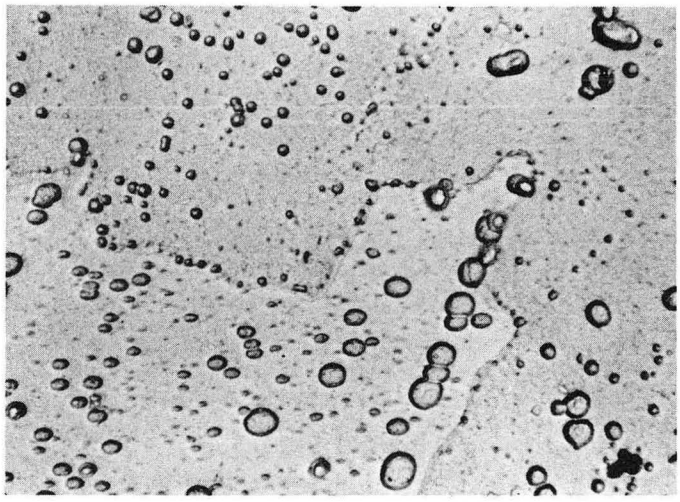

1000×

Keller's etch

XBB 679-5482

Fig. 20. Structure of fully precipitation hardened 7075-T6 aluminum alloy as revealed by the optical microscope.

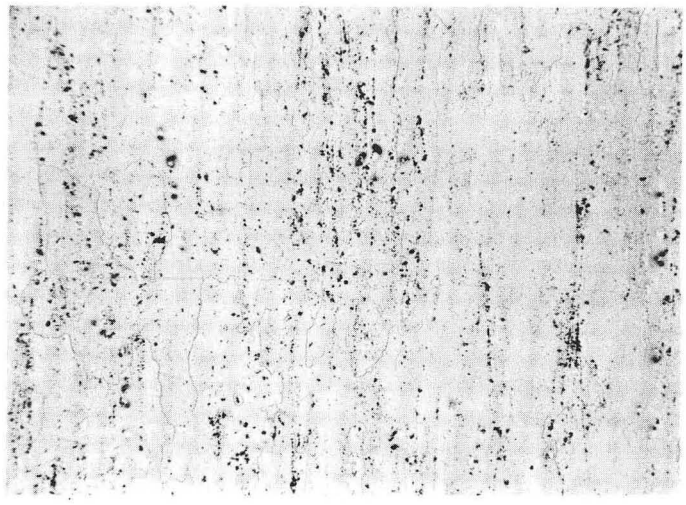

63×

Keller's etch

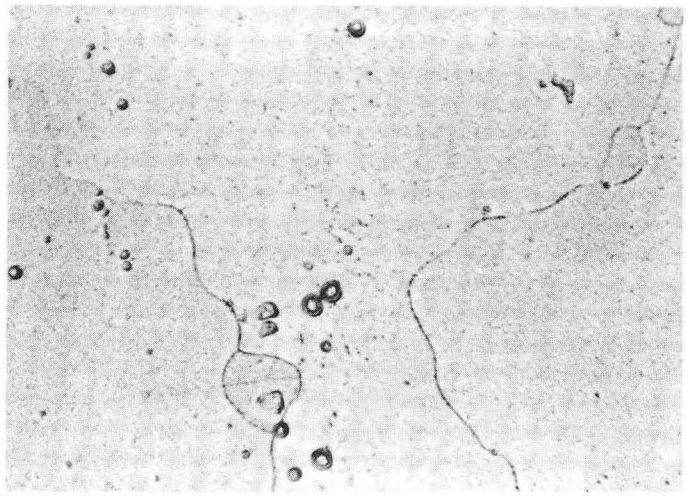

1000×

Keller's etch

XBB 679-5483

Fig. 21. Structure of underaged 7075-T6 aluminum alloy from test series 2 as revealed by the optical microscope.

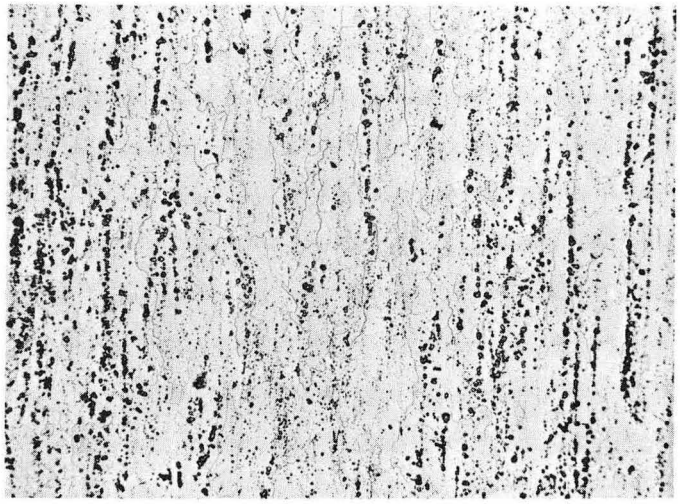

63X

Keller's etch

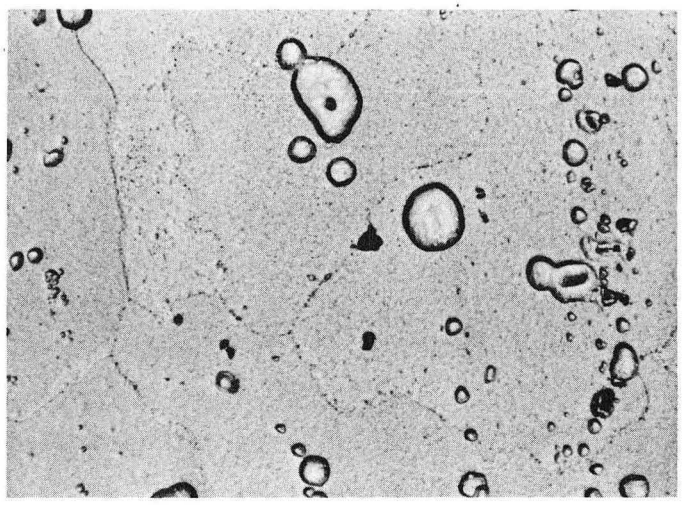

1000X

Keller's etch

XBB 679-5481

Fig. 22. Structure of overaged 7075-T6 aluminum alloy from test series 2 as revealed by the optical microscope.

This report was prepared as an account of Government sponsored work. Neither the United States, nor the Commission, nor any person acting on behalf of the Commission:

A. Makes any warranty or representation, expressed or implied, with respect to the accuracy, completeness, or usefulness of the information contained in this report, or that the use of any information, apparatus, method, or process disclosed in this report may not infringe privately owned rights; or

B. Assumes any liabilities with respect to the use of, or for damages resulting from the use of any information, apparatus, method, or process disclosed in this report.

As used in the above, "person acting on behalf of the Commission" includes any employee or contractor of the Commission, or employee of such contractor, to the extent that such employee or contractor of the Commission, or employee of such contractor prepares, disseminates, or provides access to, any information pursuant to his employment or contract with the Commission, or his employment with such contractor.